

AD-A092 527

AIR FORCE INST OF TECH WRIGHT-PATTERSON AFB OH
A WAVELENGTH MODULATED, CONTINUUM EXCITED FURNANCE ATOMIC FLUOR-ETC(U)
1980 T F WYNN

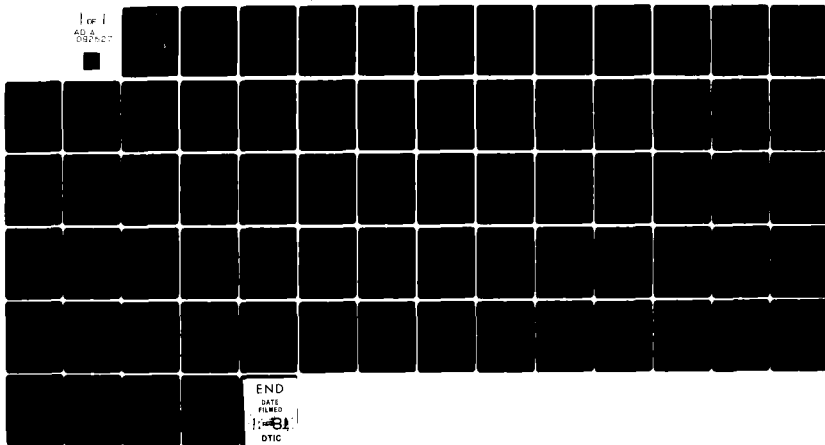
F/G 11/8

UNCLASSIFIED

AFIT-CI-80-8T

NL

1 OF 1
AD-A
092527



END
DATE
FILMED
DTIC

AD A092527

UNCLASS

SECURITY CLASSIFICATION OF THIS PAGE (When Data Entered)

LEVEL II

①

REPORT DOCUMENTATION PAGE

READ INSTRUCTIONS
BEFORE COMPLETING FORM

1. REPORT NUMBER 80-8T	2. GOVT ACCESSION NO. AD-A092 527	3. RECIPIENT'S CATALOG NUMBER
4. TITLE (and Subtitle) / A Wavelength Modulated, Continuum Excited Furnace Atomic Fluorescence System For The Determination Of Wear Metals In Jet Engine Lubrica- ting Oils		5. TYPE OF REPORT & PERIOD COVERED THESIS/DISSERTATION
7. AUTHOR(s) Thomas F. Wynn, Jr, Capt, USAF		6. PERFORMING ORG. REPORT NUMBER
9. PERFORMING ORGANIZATION NAME AND ADDRESS AFIT STUDENT AT: University of Florida		8. CONTRACT OR GRANT NUMBER(s)
11. CONTROLLING OFFICE NAME AND ADDRESS AFIT/NR WPAFB OH 45433		10. PROGRAM ELEMENT, PROJECT, TASK AREA & WORK UNIT NUMBERS
14. MONITORING AGENCY NAME & ADDRESS (If different from Controlling Office)		12. REPORT DATE 1980
		13. NUMBER OF PAGES 66
		15. SECURITY CLASS. (of this report) UNCLASS
		15a. DECLASSIFICATION/DOWNGRADING SCHEDULE
16. DISTRIBUTION STATEMENT (of this Report) APPROVED FOR PUBLIC RELEASE; DISTRIBUTION UNLIMITED		
17. DISTRIBUTION STATEMENT (of the abstract entered in Block 20, if different from Report)		
18. SUPPLEMENTARY NOTES APPROVED FOR PUBLIC RELEASE: IAW AFR 190-17 <i>Fredric C. Lynch</i> FREDRIC C. LYNCH, Major, USAF Director of Public Affairs Air Force Institute of Technology (ATC) Wright-Patterson AFB, OH 45433		
19. KEY WORDS (Continue on reverse side if necessary and identify by block number)		
20. ABSTRACT (Continue on reverse side if necessary and identify by block number) ATTACHED		

DTIC
ELECTE
DEC 05 1980
E

DDC FILE COPY

A WAVELENGTH MODULATED, CONTINUUM EXCITED FURNACE ATOMIC
FLUORESCENCE SYSTEM FOR THE DETERMINATION OF WEAR
METALS IN JET ENGINE LUBRICATING OILS

By

THOMAS F. WYNN, JR.

Accession For	
NTIS GEM&I	<input checked="checked" type="checkbox"/>
DDC T/LB	<input type="checkbox"/>
Unannounced	<input type="checkbox"/>
Justification	
By _____	
Distribution/ _____	
Availability Codes	
Dist.	Availand/or special
A	

A THESIS PRESENTED TO THE GRADUATE COUNCIL OF
THE UNIVERSITY OF FLORIDA IN
PARTIAL FULFILLMENT OF THE REQUIREMENTS FOR
THE DEGREE OF MASTER OF SCIENCE

UNIVERSITY OF FLORIDA

198C

ACKNOWLEDGEMENTS

The author thanks Dr. J. D. Winefordner for the unique opportunity to work with his research group. Further thanks are extended to the group members themselves for all the assistance offered.

In particular, the author appreciates the long hours and expert advice donated by John Bradshaw and the personal attention given by Jim Bower, Ed Voightman and Dave Bolton.

Additionally, the author points out that this study would not have been possible at all without the support, understanding and patience of his wife, Deborah.

TABLE OF CONTENTS

	Page
ACKNOWLEDGEMENTS -----	ii
ABSTRACT -----	iv
CHAPTER	
I INTRODUCTION -----	1
II HISTORICAL -----	4
III THEORY -----	9
AFS Expressions -----	9
Wavelength Modulation-S/N Considerations ----	13
Limit of Detection, Sensitivity and Precision-	14
IV EXPERIMENTAL -----	16
Apparatus and General Layout -----	16
Wavelength Modulation System -----	16
Atomizer and Optical Transistor Mounts ----	18
Temperature Calibration With The Optical Transistors -----	19
Optically Triggered Gated Integrator ----	20
Standards -----	21
Experimental Procedures -----	21
V RESULTS -----	23
VI DISCUSSION -----	24
VII TABLES AND FIGURES -----	26
VIII CONCLUSIONS AND FUTURE WORK -----	55
APPENDICES	
A WAVELENGTH MODULATOR SCHEMATIC -----	56
B OPTICALLY-TRIGGERED GATED INTEGRATOR SCHEMATIC-	58
LITERATURE CITED -----	63
BIOGRAPHICAL SKETCH -----	66

Abstract of Thesis Presented to the Graduate Council
of the University of Florida in Partial Fulfillment of the
Requirements for the Degree of Master of Science

A WAVELENGTH MODULATED, CONTINUUM EXCITED FURNACE ATOMIC
FLUORESCENCE SYSTEM FOR THE DETERMINATION OF WEAR
METALS IN JET ENGINE LUBRICATING OILS

By

Thomas F. Wynn, Jr.

March, 1980

Chairman: James D. Winefordner
Major Department: Chemistry

A historical review is presented of atomic fluorescence, continuum excitation and furnace atomization as they apply to wear metal determination in oils. The theories applicable to atomic fluorescence with a continuum source, wavelength modulation, signal to noise considerations and limits of detection are briefly presented.

A system for the measurement of atomic fluorescence is described that consists of an electrically-heated graphite filament and flame ($\text{Air/C}_2\text{H}_2$ or $\text{N}_2\text{O/C}_2\text{H}_2$) atomizer with 300-W Eimac xenon arc continuum excitation source, a wavelength modulated background connection system and an optically triggered electronic integrator. This system analyzes small volume (1 μl) of lubricating oil quickly and with no pretreatment.

Real jet lubricating oils are analyzed for Cu, Mo and Al and the determinations are evaluated with respect to the accuracy and repeatability criteria of the Joint Oil Analysis Program.

Sources of errors are discussed along with recommendations for future work.


Chairman

CHAPTER I INTRODUCTION

The purpose of the analysis of wear metals in engine lubricating oils is to diagnose impending engine failures and thus prevent possible aircraft or personnel loss. The basic premise that this approach is based upon is that all metals found in a lubricating oil sample come from the deterioration of oil-wetted metallic parts in the engine caused by friction, heat or chemical action. Further, it is assumed that the metal concentration in the oil as a function of time is a direct representation of the wear rate of the engine component containing the metal (1). For example, Figure 1 represents a typical wear metal versus time curve at the top with the corresponding wear rate curve below. The equivalent wear rate plot is obtained by differentiation of the upper plot. Focusing on the upper plot, notice the sharp rise of the metal concentration from A to B during initial break-in of the engine part. Changing of this oil drops the concentration at point C to a low level which remains nearly constant until point D. Notice that the differential curve from C to D is constant and indicates no wear, i.e., normal operating conditions. After point D, the metal concentration rises sharply, with a corresponding increase in the wear rate and an impending failure can be predicted. This time-dependent trend analysis is the basis of modern aircraft oil monitoring programs (1, 2). Records are kept for each engine on each aircraft and any marked change in any metal concentration is noted and the maintenance section is alerted for possible engine failure.

Further information may be obtained by noting which metals increase in concentration. For example, Table 1 lists the major metal present in some of the alloyed components of the J-79 and J-69 engines. Note that in many cases, a particular metal may be traced to a specific engine component. A sudden increase in Cr content of lubricating oil from a J-79 engine, for example, is most likely from the main bearing seals. This information can save a great deal of time and money when troubleshooting an engine. To provide this information, the analytical technique must have multi-element capability for all of the metals in the engine.

More generally, for an analytical technique to support an on-going routine wear metal trend analysis program, it must meet the following criteria:

- (i) Be fast enough to allow real-time input into the maintenance section prior to actual failure of the engine;
- (ii) Be simple enough to be operated by technicians with no scientific background (2); and
- (iii) Be capable of accurate multi-element determinations of metals over a wide concentration range in an extremely complex matrix.

The first two requirements imply an analytical procedure which requires little or no pretreatment of the oil samples and one which is adaptable to automated control.

The third requirement is the most difficult to solve. Used engine oil is extremely viscous and normally opaque. Oil volatility, smoking and flashpoint characteristics can obscure an analyte signal. Further, the metals of interest are present with many others and spectral line overlap may present resolution problems.

In this study, a carbon filament atomizer is used to effect the atomization of oil samples without pretreatment. This is due to the capability of a separate ashing step. In addition, the timing cycles

are easily automated, simplifying the procedure and reducing the time of analysis. The filament was placed in an Ar-sheath during the ashing and cooling cycles to prolong filament life and to provide an inert atmosphere. During the atomization cycle, a flame surrounds the filament to minimize cooling of atomized metals and forming of refractory compounds prior to excitation. This is especially important for those elements requiring high atomization temperatures.

Atomic fluorescence spectrometry (AFS) is the method of choice for the determination of the metal concentrations, due to the wide linear range and high sensitivity. By employing a continuum source, multi-element analysis is possible with the addition of a direct reader, although this aspect was not a part of this study.

To complete this system, a wavelength-modulation with a lock-in amplifier is used to improve the S/N ratio, and an optically-triggered integrator is installed to improve reproducibility. Both of these methods aid in extraction of signals from intense backgrounds.

Specific aspects of these methods will be discussed further in the section on the theory.

CHAPTER II HISTORICAL

Nearly every analytical technique imaginable has been employed for monitoring wear metals in lubricating oils. Routine methods employed include (1): ferrography, x-ray fluorescence, capacitance measurements, electron probe microanalysis and magnetic plug inspection. Some of the non-routine methods used are: mass spectrometry, electron spin resonance, Mössbauer spectroscopy, scanning electron microscopy and various methods for the measurement of physical properties of the oil itself.

The most important of the monitoring techniques are the various spectroscopic techniques, collectively called the Spectrometric Oil Analysis Program (SOAP) by the U. S. Air Force. The railroads, airlines, U. S. Navy and the U. S. Air Force all have active SOAP programs, the military program dating from 1955 (3,4). The U. S. Navy and Air Force are both monitored by a single agency termed the Joint Oil Analysis Program (JOAP) (5).

Currently, the U. S. Air Force SOAP consists of approximately 120 SOAP laboratories located worldwide (3). Of these, the majority (approximately 80) employ an atomic-emission-spectrometric system with a rotating carbon disk electrode AC spark excitation source and a direct reading spectrometer (2,5). The remaining laboratories use flame atomic absorption systems; however, it is reported that the Air Force is considering converting these to the emission system, since the atomic absorption set up requires sample dilution, whereas the

emission device does not (2,3,4,5). The emission device is capable of a large number of determinations: Na, Zn, V, Mo, Mg, Cd, Ba, Bo, Ti, Sn, Si, Pb, Ni, Na, Mg, Cu, Cr, Be, Al, Ag, Fe (2). On a routine basis, however, only approximately half of these elements are determined, depending on the aircraft type from which the oil sample was taken. For example, the SOAP laboratory at MacDill AFB, FL., calibrated their spark emission spectrometer only for Fe, Ag, Al, Cr, Cu, Mg, Ni, Si and Ti and of these makes routine determinations only of Al, Fe, Cu, Ag, Mg and Ti. Of further interest is the fact that the metal determinations are recorded only to the nearest ppm, i.e., anything less than 1 ppm is recorded as zero (2,4).

Atomic fluorescence spectroscopy (AFS) as a means of chemical analysis was introduced in 1964 by Winefordner and Vickers (6) and by Winefordner and Staab (7) and in 1966 by Dagnall, West and Young (8).

The use of a continuum source for AFS was first reported by Veillon et al. in 1966 (9). The authors used a 150-W xenon arc lamp of the Osram type and a DC electrometer for AFS studies. Further work was carried out by Ellis and Demers (10), Dagnall et al. (11) and Manning and Heneage (12). In 1970, Bratzel et al. evaluated the 150-W Eimac xenon arc lamp for AFS (13). The authors pointed out that the xenon arc lamps are generally cheaper, more stable and longer lived than other AFS sources and they can be used for multielement analysis. In addition, analytical curves can be predicted accurately with continuum sources. Bratzel demonstrated the potential of the Eimac for multielement analysis. Cresser and West (14) employed a 500-W xenon arc lamp for the determination of 13 elements. Fowler and Winefordner (15) studied the background in AFS observed with an Eimac lamp and recommended wavelength modulation to reduce broadband fluorescence scatter and source flicker.

The application of AFS to oil analysis for wear-metals was first investigated by Smith et al. (16) in 1969. The authors used electrodeless discharge lamps (EDL) for sources and a total consumption burner with an H_2 /Ar/entrained air or H_2 /entrained air flames for atomization. Satisfactory results were obtained for six elements in oil samples. With the H_2 /air flame, dilution of the oil (10:1) with methyl isobutyl ketone was required.

Miller et al. (5) used a 150-W Eimac xenon arc lamp as an excitation source and a total-consumption burner with an H_2 /Ar/air flame for AFS in oil samples. Again, oil samples were diluted (4:1) with CCl_4 prior to use.

Johnson, Plankey and Winefordner (17) employed AFS with a pulsed xenon arc lamp and a CW xenon arc lamp with a special mirror system enabling the transfer of nearly all the radiation produced by the lamp into the flame (air/ C_2H_2 or N_2O/C_2H_2) atomizer. They concluded that the CW Eimac produced better limits of detection (LOD) than the pulsed source. In addition, the pulsed lamp had a limited lifetime.

Later, Johnson et al. (18) used a similar instrumental set up but employed a chopped 150 W Eimac excitation source for the AFS study of primary SOAP standards. They obtained data for Ag, Cr, Cu, Fe, Mg, Ni and Pb with no pretreatment of the oil samples.

In 1975, the same authors (19) added a computer-controlled, slewed-scan spectrometer for multielement analysis. Fe, Mg, Cu, Ag and Cr were determined.

The graphite atomizer began to appear in oil analysis in 1971 when Brodie and Matousek (20) employed a graphite mini-Massmann furnace to directly determine Ag, Al, Cu, Cr, Mg, Ni and Pb in lubricating oils.

The higher viscosity oils were diluted with xylene prior to use. The average relative standard deviation was reported to be less than 4%. About the same time, Alder and West (21) used a carbon filament in an Ar sheath to directly determine Ag and Cu in 1 μ l lubricating oil samples with both AFS and atomic absorption spectrometry (AAS). Omang (22) used a graphite tube furnace to determine Ni and V in crude petroleum.

In 1979, the flame and furnace were combined by V. P. Borzor et al. (23, 24). The authors described the use of a carbon rod filament atomizer in an air/C₂H₂ flame to determine Cu in various matrices. The use of the flame was to prevent rapid cooling of the atomized analyte species above the filament. Later, Amos (25) used a carbon rod atomizer which was enclosed in an H flame. In 1972, Molnar et al. (26) developed a similar electrically heated graphite filament which was operated in an H₂/Ar/entrained air flame. The atomizer was used for AAS of Ag, Cu and Fe in oil samples diluted (10:1) with isooctane.

Reeves et al. (27) used the same atomizer for AAS determinations of Ag, Cr, Cu, Fe, Ni, Pb and Sn in jet and reciprocating oils. USAF SOAP correlation samples were analyzed with excellent agreement for Ag, Cu, Fe, Ni and Pb. Chuang and Winefordner (28) and Chuang et al. (29) used the same atomizer for AAS studies of Ag, Cu, Fe, Mg, Ni, Pb and Sn in USAF SOAP samples with excellent agreement for all elements studied.

Patel et al. (30) in 1973 applied the same atomizer for AFS studies. They obtained data for Ag, Pb and Sn in SOAP organometallic standards. Patel and Winefordner (31) also used this atomization set up with a multielement EDL to determine simultaneously Ag and Cu in jet engine oils, both standards and SOAP correlation samples, with good results.

In 1976, Katskov, Kruglikova and L'vov (32) reported the use of a resistively heated graphite chamber in an air/C₂H₂ or N₂O/C₂H₂ flame with AAS. Determinations of 27 elements, including Ti, V, Mo and Si in many matrices including oil. Later, the same atomizer was used by Razumov (33) for AAS and AFS studies.

The work which precipitated this present study was conducted in 1978 by Vaughn (34). They employed the same graphite rod furnace described by Molnar et al. (26), except that the burner system was modified to accept a circular burner head in the center of the block for an air/C₂H₂ or a N₂O/C₂H₂ flame with an argon outer sheath. Determinations of Cr, Al and Mo in SOAP oil correlation samples and aqueous samples by AFS with chopped Eimac 150-W source. Moderate agreement (50%) with the USAF SOAP correlation samples was reported with limits of detection in oil of 0.4 ppm for Cr, 0.3 ppm for Al and 1.0 ppm for Mo.

This study employed the same graphite rod-burner device, but replaced the mechanical chopper with an electronically-controlled wavelength modulator and added two optical transistors, one to trigger an electronic integrator, the other to measure temperature of the filament. AFS was conducted with USAF oil correlation samples for Cu, Mo and Al. Specific differences are discussed in the experimental section.

CHAPTER III THEORY

AFS Expressions

If we assume a sample cell is illuminated along a length L and observed at right angles along length l (see Figure 2), there are four possible illumination and observation profiles as depicted in (a), (b), (c), (d) (35). Case (b) depicts a cell that is incompletely illuminated and the fluorescence of the illuminated portion is absorbed by the unilluminated portion, called post filter effect or self-reversal. Case (c) is a cell that is fully illuminated, however, only a portion is observed, termed pre-filter effect. Case (d) is a combination of the two. Case (a) is the idealized case, where the cell is completely illuminated and observed along the entire length. In this case, the only attenuation effect on the fluorescence emission is self-absorption.

If case (a) is assumed, then in general the radiance of any fluorescence transitions can be expressed by (35):

$$B_F = \left(\frac{1}{4\pi} \right) A_{ul} h\nu_o n_u \left[\frac{A_t^*(l)}{\int_0^l k^*(\nu) d\nu} \right]$$

where: B_F = radiance, $J s^{-1} m^{-2} Sr^{-1}$;

A_{ul} = Einstein coefficient of spontaneous emission, photons s^{-1} of excited species;

$h\nu_o$ = energy of transition, J;

n_u = concentration of upper level, m^{-3} ;

$k^*(\nu)$ = net absorption coefficient accounting for induced emission, m^{-1} ;

$A_t^*(l)$ = total absorption or equivalent line width as a function of l , Hz;

The term in the large brackets accounts for the self absorption effect. A more specific expression for a continuum source and for low optical density is

$$B_{FC} = \left(\frac{2h\nu_o^3}{c^2} \right) \left(\frac{Y}{L A_{ul}} \right) \left(\frac{1}{h\nu_o} \right) \left(\frac{A_{ul} \lambda_o^4}{8 \pi c} \right) \ell L E_{C\lambda_o} \int_0^\infty k^*(\lambda) d\lambda$$

or for high optical density is

$$B_{FC} = \left(\frac{2h\nu_o^3}{c^2} \right) \left(\frac{Y}{L A_{ul}} \right) \left(\frac{1}{h\nu_o} \right) \left(\frac{A_{ul} \lambda_o^4}{8 \pi c} \right) \frac{\left(\delta\lambda_D \sqrt{\frac{\pi^{1/2} k_o \ell a}{\ln 2}} \right) \left(\delta\lambda_D \sqrt{\frac{\pi^{1/2} k_o L a}{\ln 2}} \right) E_{C\lambda_o}}{\frac{\pi^{1/2} k_o \delta\lambda_D}{2 \sqrt{\ln 2}}}$$

$$= \left(\frac{2h\nu_o^3}{c^2} \right) \left(\frac{Y}{L A_{ul}} \right) \left(\frac{1}{h\nu_o} \right) \left(\frac{A_{ul} \lambda_o^4}{8 \pi c} \right) \frac{2 \sqrt{a}}{\sqrt{\pi^{1/2} k_o n f L}}$$

where

$$\frac{Y}{L A_{ul}} = \text{number of excited species/photon, } s^{-1} m;$$

$$E_{C\lambda_o} = \text{spectral irradiance of the continuum source, } J s^{-1} m^{-2};$$

$$\delta\lambda_D = \text{Doppler half-width of the fluorescence line, } m; \text{ and}$$

$$a = \text{damping constant, dimensionless.}$$

$$k_o = \text{the peak absorption coefficient for Doppler broadening, } m^{-1}$$

A correction for post filter effect can be represented by (36):

$$F_{po} = \frac{A_t (\ell + \Delta\ell)}{A_t (\ell)} \frac{(\Delta\ell)}{\ell} \quad \text{and, if } \xi = \frac{\Delta\ell}{\ell},$$

$$F_{po} = \frac{A_t(\ell[\xi + 1]) - A_t(\ell\xi)}{A_t(\ell)}, \text{ further}$$

$F_{po} = 1$ at low optical density, or

$$F_{po} = \sqrt{\xi + 1} - \sqrt{\xi} \quad \text{at high optical density.}$$

The pre-filter effect correction is (36):

$$F_{pr} = \frac{A_t(L + \Delta L) - A_t(\Delta L)}{A_t(L)} \quad \text{and if } \psi = \frac{\Delta L}{L}$$

$$F_{pr} = \frac{A_t(L[\psi + 1]) - A_t(L\psi)}{A_t(L)}$$

and

$F_{pr} = 1$ if at low optical density or

$$F_{pr} = \sqrt{\psi + 1} - \sqrt{\psi} \quad \text{if at high optical density.}$$

For practical applications, an instrumental constant k should be included, which converts radiant flux incident upon the monochromator entrance slit into photomultiplier (PM) detector signal (37).

From these intensity relationships, the shape of the analytical curves of growth can be predicted. For a given atom, line and flame, the quantities a , Y , $\delta\lambda_D$, L , ℓ and k_o are constant. For a given source, $E_{C\lambda_o}$ is constant. Only a and Y are moderately dependent on flame temperature and flame composition. In the ideal case, it can be shown that (37) B_{AFC} is directly proportional to n and the $\log B_{AFC}$ vs $\log n$ plot should be linear with a slope of 1 at low optical densities and 0.0 at high optical densities. Note, however, that neither case can be applied to an intermediate region. Prefilter and post filter effects cause B_{AF} to be smaller than expected.

Winefordner (38) related the peak atomic concentration n in atoms cm^{-3} of analyte in a graphite cell to the analyte concentration c in moles/l introduced into the cell by:

$$n = 6 \times 10^{20} v c_{\epsilon} \beta / v_c$$

where:

v = volume of solution, cm^3 ;

ϵ = degree of aspiration, dimensionless;

β = degree of atomization, dimensionless; and

v_c = internal volume of the cell, cm^3 .

Further, the major advantage of a graphite furnace, which is the ability to atomize extremely small samples, is demonstrated by a ratio of the above expression to a similar one for flames. The result is

$$R = 60 [(v/v_c) (\epsilon\beta)_G / (F/Qe_F) (\epsilon\beta)_F]$$

where

Q is the flow rate of the unburnt gases into the flame in $\text{cm}^3 \text{s}^{-1}$; and e_F is the gas expansion factor for the flame. Subscript G indicates graphite furnace, subscript F indicates flame.

Typical values substituted into this ratio give $R = 600$. This can be explained by the smaller expansion of the analyte in furnaces, and $(\epsilon\beta)_F$ is usually less than unity.

It should be pointed out that the analyte concentration over the filament is a complex time-dependent function; factors involved include: samples size; analyte concentration in the sample; porosity of filament; area of coverage; temperature of the filament; the temperature rise time of the filament; the atomizing temperature of the analyte; matrix interferences; and other factors.

Wavelength Modulation - S/N Considerations

Wavelength modulation refers to the technique where the wavelength is oscillated over a small spectral interval, $\Delta\lambda$, centered on some λ_0 of interest. This produces an AC signal which is normally demodulated by a lock-in amplifier. A graphical representation is presented in Figure 3 (39). If the $\Delta\lambda$ is centered on λ_0 , the frequency of the resulting AC signal is $2f$, where f = modulation frequency. A much larger signal is obtained by getting $\Delta\lambda$ slightly off the peak and the resulting signal is at $1f$. Notice that at $1f$, a single scan is an approximation of the first derivative, while the $2f$ is an approximation of the second derivative (see Figure 4) (40). These are only approximations due to the large $\Delta\lambda$ in relation to the line width. It can be assumed, therefore, that a $1f$ signal is the best selection when the analyte line is amidst a relatively flat background. Note that if there is a sloping background, however, the $1f$ mode will give an erroneous signal. This will not occur in the $2f$ mode, as long as the background is broad-band, with no peaks in the $\Delta\lambda$ region. Epstein and O'Haver (41) have demonstrated this experimentally.

The lock-in amplifier employs a phase-sensitive detector to compare input signals with the reference frequency $1f$ or $2f$ of the oscillator. Figure 5 (42) graphically illustrates the dc output of a lock-in if the input signal is in phase with the reference i.e., $\theta=0^\circ$. Figure 6 shows the effect of a $\theta=90^\circ$ signal input. Notice the output is zero. If the signal input is 180° out of phase, Figure 7 demonstrates the negative output. Phases other than 0° , 90° and 180° give intermediate results.

Thus, for a PM detection system, if the phase is set up so that the analyte signal is in phase with the reference signal, only light in phase with the analyte will give the maximum dc output. All other sources of interferences that are not in phase with the analyte signal will give a negative (opposite polarity) dc output or at worst a smaller positive polarity output. This accounts for the ability of the lock-in amplifier to extract signals from large noise backgrounds.

To compare wavelength modulation with other modulation methods, e.g. amplitude modulation (AM), sample modulation (SM) and unmodulated continuous wave (CW), a general S/N ratio for luminescence signals, S_L , with differing parameters for each method was presented by Boutilier et al. (43) and is reproduced here in Table 2. Notice that the WM method offers an improvement in scatter source flicker noise, interference luminescence flicker and analyte flicker over the AM treatment. None of the modulation techniques offer improvement in the case of shot noise.

In the operation of a filament furnace, variable atomization rates cause a loss of precision. Several authors (24, 44) have recommended the use of an integrator to improve precision. In addition, an optical trigger, as employed, gives more reproducible triggering, reduced drift and further improved precision.

Limit of Detection, Sensitivity and Precision

In this study, any reference to sensitivity refers to the slope of the calibration curve S , i.e., the slope of a plot of c versus signal.

Further, as is customary, the standard deviation is

$$s = \sqrt{\sum_{i=1}^n \frac{(x_i - \bar{x})^2}{n-1}} \quad \text{where } \bar{x} \text{ is the mean of } n \text{ measurements.}$$

and the precision is represented by the relative standard deviation

(RSD):

$$RSD = \frac{s}{\bar{x}} \quad \text{or} \quad \%RSD = \frac{s}{\bar{x}} \times 100$$

The limit of detection is defined (45) as:

$$C_L = \frac{\bar{x}_L - \bar{x}_b}{s}$$

where \bar{x}_L is the limiting detectable measure including the blank, and

\bar{x}_b is the mean blank measurement. So:

$$\bar{x}_L = \bar{x}_b + ks_b$$

where k is a protection factor and s_b is the standard deviation of the blank. Normally, k is defined as 3, therefore the practical expression

is
$$C_L = \frac{3s_b}{s} .$$

This corresponds to a practical confidence level of 90%. Also the RSD is about 0.5 at the LOD.

All of these expressions are consistent with IUPAC (46) as published in 1978.

CHAPTER IV EXPERIMENTAL

Apparatus and General Layout

A schematic depicting the experimental set up is shown in Figure 8. Instrumentation and parameters are given in Table 3. Asterisks mark the additions and changes made to the experimental set up as studied by Vaughn (34) and are discussed at length below.

Optical alignment was accomplished through the use of a Spectra-Physics He-Ne laser, the Eimac lamp was focused to a spot 5 mm in dia 4 mm above the center of the filament with the geometry as depicted in Figure 8. Not shown is an improved light trap (Figure 9), machined from aluminum and painted flat black, that fits over the burner head. A second, larger light trap (Figure 10) was used to shield the area between the burner and the monochromator from other light in the room.

Wavelength Modulation System

The wavelength modulator used in this study was designed by Epstein and O'Haver (41) and constructed locally by Epstein. The system consisted of three units: a torque motor oscillated plate within the monochromator, an 80 Hz function generator (oscillator) used to reference the lock-in and drive the torque motor amplifier. Figure 11 depicts schematically the layout of these components. The electrical schematics of the function generator and the torque motor drive amplifier are depicted in Appendix A.

By adjusting the $\Delta\lambda$ control potentiometer on the function generator, the $\Delta\lambda$ interval could be adjusted from 0 to $3\overset{\circ}{\text{A}}$ maximum $\Delta\lambda$. A calibration curve was constructed in Figure 12 depicting optimum $\Delta\lambda$ interval versus

slit width. These values were obtained by Epstein and were confirmed during the course of this work.

In their previously mentioned work (41), Epstein and O'Haver presented a method for estimating $\Delta\lambda$ by centering a monochromator on a line, taking the PM tube output directly to an oscilloscope that had as the horizontal axis the modulating frequency and varying $\Delta\lambda$ until the line shape showed no tailing. Figure 13 depicts the resulting display for three cases. Case (a) represents a large $\Delta\lambda$, i.e., $\Delta\lambda \gg 2s$, where s is the spectral bandpass of the monochromator. If $\Delta\lambda$ is narrowed until the tailing or background is removed, $\Delta\lambda = 2s$, and this is the optimum on-the-peak or 2 f modulation case, shown in (b). The last case (c) is where $\Delta\lambda = 1s$ and 2 f signal is at a minimum, 1 f signal is at a maximum. This technique is extremely useful for setting up on a particular line. Using this technique, an optimum slit width setting of 100 μm and a $\Delta\lambda$ of 2.4 \AA was determined.

The monochromator can be further fine-tuned on the line by employing the lock-in amplifier phase angle adjustment. Notice that by varying the phase angle from 0 to 360°, the output is the same as if the monochromator had been scanned from $\lambda_0 - \Delta\lambda$ to $\lambda_0 + \Delta\lambda$ (refer to Figure 3). So, in the first derivative mode, i.e., at 1 f on the lock-in, the signal will cross zero at the actual peak of the line. This will also correspond to the maximum 2 f signal. Figure 14 is a typical plot of a HCL signal versus phase angle for both 1 f and 2 f when the monochromator is set on the peak. As expected, the 1 f signal is small compared to the 2 f signal. Also notice that to ensure the correct phase angle for maximum signal once the zero point of the 1 f has been determined, the phase angle in the 2 f mode is adjusted to zero and then exactly

$\pm 90^\circ$. Note from Figure 14 that this will guarantee the maximum 2 f signal. This is the technique that was routinely employed for setting up on a line, and for adjusting for monochromator drift during measurements.

Atomizer and Optical Transistor Mounts

The atomizer (see Figure 15) consisted of a cylindrical bakelite block 8.2 cm in diameter and 2.6 cm high with water cooled blocks on either side which were electrodes and supports for the filament. The graphite filaments were machined locally from 0.254 in diameter rods from the stock listed in Table 4 to the dimensions depicted in Figure 16. The filament was held in place and electrical contact made through set screws in the copper blocks.

An aluminum block with 56 holes 1.3 mm in diameter was inserted in the block to entrain an Ar sheath around the filament. A capillary burner, consisting of 83 capillary tubes 1.0 mm inside diameter and 3.8 cm long supported the N_2O/C_2H_2 or air/ C_2H_2 flame.

As mentioned earlier, two optical transistors were employed in this system, one for optical triggering and one for temperature measurements. To insure reproducibility, it was decided to permanently mount the optical transistors in the bakelite block with the lens permanently fixed on the center of the filament. Figure 17 illustrates the brass holder design which both held the transistor in a permanent position and provided a means for attenuation of the filament radiation intensity to useable levels. In Figure 17 (a), the lower temperature cap is depicted. This cap was used for low temperature measurements and to trigger the integrator. The neutral density filter was 1/8 in thick. In Figure 17 (b), the higher temperature cap is shown. The 1/64 in hole through 1/8 in

of brass gave excellent attenuation and did not require a filter. This cap was used for higher temperature measurements.

The mounting channels in the bakelite block are depicted in Figure 18 (a) and (b). Notice the transistor holder is recessed in the bakelite for temperature protection. After several months, the bakelite burned away (especially when using the N_2O/C_2H_2 flame) and exposed the holder and the cap had to be shortened to allow further recess. Eventually, a mica window was placed over the holder to protect from the extreme temperature. Otherwise, a long cooling period was required before the transistor would function properly again.

Temperature Calibration With The Optical Transistors

One of the primary reasons for the use of the optical transistors was to obtain fast estimate of temperatures. Vaughn (34) noted that as a filament aged, the temperature rose even though the programmer settings had not been adjusted. This was because the diameter became smaller as the filament oxidized and the resistance therefore increased. Since an optical transistor reads intensity directly, a good estimate of the temperature can be made instantly, regardless of the age of the filament.

To accomplish this end, a biasing circuit was built (Figure 19) that gave an output at V_{out} that was proportional to the current across R_L , and the current through the transistor is proportional to the intensity of the light impinged upon it; R_L was adjustable to allow a change in the temperature measurement range.

Calibration was carried out with the set-up shown in Figure 20; the voltage output of the bias circuit was compared to the temperature readout of a W-W/26% Rh thermocouple (Omega engineering, Inc. Stamford,

Conn. 06907). For temperatures above the thermocouple limit (2300°C), an optical pyrometer was used. The resulting calibration curves are given in Figure 21. These curves became extremely important for monitoring filament temperatures when determining Mo and Al due to the higher atomization temperatures involved.

Optically Triggered Gated Integrator

The second optical trigger was used to trigger the gated integrator, a locally-designed and constructed instrument (47). The electrical schematic is given in Appendix B. The integrator had provisions for a temperature adjustment to control the threshold of the trigger, a delay time adjustment that allowed a delay between the trigger pulse and the beginning of the gate, and a gate time adjustment. The setting of these two parameters was critical for precision. For example, Figure 22 is a typical oscilloscope trace for a copper fluorescence. Notice the gate is set so that $\tau_{\text{delay}}=0$ and that τ_{gate} is set to approximately where the signal returns to the baseline. It is obvious that any significant τ_{delay} would chop off the first part of the peak. Also, τ_{gate} must be long enough to include all of the peak, but not so long as to greatly reduce sensitivity. An even more important example is shown in Figure 23, a trace of 50 ppm of Mo in a $\text{N}_2\text{O}/\text{C}_2\text{H}_2$ flame. Since the most sensitive line of Mo is at 313.2 nm, OH interference from the flame is intense. In addition, the Mo is atomized more slowly. The result is that initially there is a negative signal (180° out of phase) until the Mo begins to atomize. It is obvious in this case that the choice of delay time can radically affect the integrated result. Also, as the filament ages, it heats more quickly and the analyte peak shifts to the left and is narrower. Therefore, as the filament ages, both

τ_{delay} and τ_{gate} must be reduced. For this reason, the output of the lock-in amplifier was continually monitored on an oscilloscope triggered with the integrator trigger and adjustments made as necessary.

Standards

Standards employed were the Special Spectrometric Calibration Standards obtained from the Naval Air Rework Facility, Naval Air Station, Pensacola, FL. These standards contain the elements Al, Cr, Cu, Fe, Pb, Mg, Ni, Si, Ag, Mo, Sn and Ti at concentrations of 3, 10, 30, 50 and 100 ppm. The base oil was Conostan 85. Standards of 0.1, 1, and 5 ppm were obtained by diluting the SOAP standards with base oil by weight. The oil correlation samples analyzed were synthetic and real samples that had been analyzed independently by the labs in JOAP and the results correlated.

Experimental Procedures

All samples were introduced with a calibrated 1 μl Micropettor A syringe (Scientific Manufacturing Industries, Emeryville, CA 94608) and the capillaries disposed of between samples. In addition, a separate Micropettor was used for the blank to prevent blank contamination.

The N_2O flame was adjusted to a red feather to help reduce oxide formation (48) with the resulting flow rates of 7.2 l min^{-1} for N_2O and 4.3 min^{-1} for C_2H_2 , gas flows measured with rotometers calibrated in l min^{-1} . The Ar flow was 2.2 l min^{-1} for the optimized signal for this system as reported by Vaughn (34).

Since oil standards were being used, ashing was a must, with temperature and time of ashing adjusted to complete smoke formation prior to atomization. Smoke during the atomization cycle resulted in huge scatter induced fluctuations which normally saturated the lock-in amplifier. Typical values were 800°C and 15s for the ashing cycle.

Attempts were made to obtain complete calibration curves, but extremely short filament lifetimes made this difficult. Therefore, all the correlation samples were determined by bracketing the unknown with standards of known concentrations. Some of the samples were determined with only one standard. In any event, all readings were paired, eg., standard-blank-unknown-blank-etc.

All integration values were obtained from the DVM. The integration gate was monitored by a light emitting diode which was illuminated during the gate cycle. The lock-in signal was monitored on the oscilloscope, as was the temperature readout of the optical transistor.

The fluorescence lines used were 324.7 nm for Cu, 313.3 nm for Mo, 394.4 nm for Al; all lines were recommended by Parson's et al. (49).

The filament temperatures for the elements were: Cu - 2300°K, Mo - 2950°K, Al - 2800°K. These were the minimum temperatures used for analysis of these elements. The values were determined by plotting a series of determinations of the same standard and increasing the temperature until the value of the concentration determination stabilized, indicating that all of the analyte had been atomized.

CHAPTER V RESULTS

The results of the oil analysis are given in Table 4. Data for Mo were obtained only for samples 193 and 194 as explained in note (c). Mechanical and electrical failures prevented completion of the analysis of 193-198 for Al. The criteria for repeatability and accuracy are determined by plotting the paired sample values and measuring if the plot falls within allotted tolerances, determined by JOAP for each pair. For example, Figure 24 illustrates the procedure for samples 183 and 184. After the JOAP trimmed mean and criteria are plotted, the experimental data obtained in this work is plotted, and it falls within the area; so samples 183 and 184 meet JOAP criteria. Figure 25 is another example for Mo.

There was enough data for Cu for a calibration curve, which is given in Figure 26. From the slope of this curve and the best blank standard deviation over five runs on a single filament, the LOD for Cu for this technique can be reported as 0.09 ppm or 9×10^{-11} g. The LOD for Mo for a single filament can be estimated to be 0.4 ppm or 4×10^{-10} g. The LOD for Al was not determined, but it is less than 1 ppm.

The high end of the linear range was not determined, since extremely large concentrations of these metals are not expected in oil samples. In any event, the linear range extends past 100 ppm for all three elements.

CHAPTER VI DISCUSSION

The results obtained in this study compared extremely well with the JOAP correlation results for both real and synthetic samples. All of the sample pairs determined met the JOAP criteria. This compares with 50% of the 6 pairs studied with the previous system by Vaughn (34). The limit of detection for Mo was approximately 50% better also. The overall RSD for the Cu runs was 5.7%, which is excellent for a graphite atomizer.

The system has great future potential due to the ease with which the system could be automated. With the optically triggered integrator and a programmed timer, the operator merely has to inject a sample, press a button and read the value directly off of a DVM. The technique definitely has potential for rapid work also, the actual analysis on the machine taking only approximately 20 s.

The major concern and the suggested area for further study is filament life and stability. This author confirmed that the filament temperature rises from run to run. In fact, when working in a $\text{N}_2\text{O}/\text{C}_2\text{H}_2$ flame, the filament often increased 300°C or more. In addition, not only did the maximum temperature increase, but the rate of temperature increase also was greater. This certainly reduced the precision considerably. A possible solution is some type of differentiating and comparator circuit which will sense a change in the slope and change the power input to keep it constant. Pyrolytic treatment of the graphite

may also improve the filament life, although the POCO FX91 is supposedly treated to $> 2500^{\circ}\text{C}$ prior to delivery. Other possibilities include a larger filament diameter, or a different shape. In any event, in the opinion of this author, filament oxidation is the major cause for loss of precision.

The small sample size also introduces uncertainty since the oil samples are not necessarily homogeneous. In fact, shaking of the oil samples is a must. Further, the metal particle size in the oil affects the result, although probably to a lesser extent with the gated integrator. For example, Saba and Eisentraut(3) point out that Mo is definitely particle size dependent.

Matrix-related interferences may include chemical interferences, occlusion of the analyte or spectral overlap. However, Krasowski and Copeland (50) point out that there is little agreement as to the primary causes of matrix interferences in furnace atomization.

Normally, with a modulated system and good electronics, electronic noise is of minimal importance. It was noticed, however, that the SCR power supply often caused oscillations of ± 0.5 V when on, and when looking at very low concentrations became the major noise source. It is suspected that RF generated by the large power surges through the lines is the cause. It is suggested that the SCR be moved and shielded prior to further study.

TABLE 1
MAJOR METAL CONSTITUENT OF ALLOYED J-69 AND J-79 ENGINE COMPONENTS

Engine: J-79 Aircraft: F-4, A-5^a

Metal	Component
Fe	Main bearing housing
Cu	Main bearing cages
Al, Mg	Main gearbox castings
Cr	Main bearing seal races
Mo	Transfer gearbox, bearing housings ^b

Engine: J-69-T-29 Aircraft: T-37^c

Cu (Ag, Sn)	Front bearing cage
Fe	Front bearing balls and races
Fe, Al (Cr)	Oil pump
Al, Mg	Accessory housing

^aTaken from USAF Technical Order TO-33-1-37, MacDill SOAP lab., p.6-37.

^bFrom C.S.Saba and K.J.Eisentraut, Anal. Chem., 51, 1927(1979).

^cFrom USAF J-69-T-29 Turbojet Engine Trouble Shooting Guide, Fig. FO-32.

TABLE 2
GENERAL SIGNAL-TO-NOISE RATIO EXPRESSIONS FOR LUMINESCENCE SPECTROMETRY
WITH DEFINITION OF TERMS

$$\frac{S}{N_L} =$$

S_L					
$\sqrt{N_{LS}^2 + N_{ES}^2 + N_{IS}^2 + N_{SS}^2 + N_{BS}^2 + N_{DS}^2 + (N_{LF} + 2^r N_{SF} + 2^u N_{IF})^2 + 2^p (N_{EF} + 2^q N_{BF})^2 + [2^w N_{DF}]^2 + [2^w N_A]^2}$					
Measurement mode	p	q	r	u	w
CW	1	1	1	1	1
AM	0	1/2	1	1	1/2
WM	1	1/2	1/2	1/2	1/2
SM	1	0	0	0	1/2

where:

- N_{ES} = analyte emission shot noise;
 N_{BS} = background emission shot noise;
 N_{DS} = detector shot noise;
 N_{LS} = analyte luminescence shot noise;
 N_{SS} = scatter (source) shot noise;
 N_{IS} = interferent (in sample/blank) luminescence shot noise;
 $2^w N_A$ = amplifier readout noise;
 N_{EF} = analyte emission flicker noise;
 $2^q N_{BF}$ = background emission flicker noise;
 $2^w N_{DF}$ = detector dark flicker noise;
 $2^r N_{SF}$ = scatter (source) flicker noise;
 $2^u N_{IF}$ = interferent (in sample/blank) luminescence flicker noise;
 N_{LF} = analyte luminescence flicker noise; and
 S_L = analyte luminescence signal.

TABLE 3
INSTRUMENTATION AND PARAMETERS

Component	Model No.	Company
Monochromator	Jarrel Ash 0.5 m, Ebert mount, Model 82-000, δ angle at 400nm, adjustable curved slits 100 μ m, 7 mm slit height	Jarrell-Ash Co., Newtonville, MA 02160
Detector	Photomultiplier tube, 900V	
Detector Power Supply	Model 402M Fluke power supply	John Fluke Mfg. Co., Seattle, WA
Amplifier	Ithaco Lock-in Synchronous Detector Model 391A with 1 f and 2 f modes, 400 ms TC	Ithaco, Ithaca, NY 14850
Preamplifier	Ithaco Model 164 with 10^4 , 10^6 , 10^8 V/A settings	
Furnace graphite	POCO Spectrographic electrode rods, grades FXI and* FX9I (FXI now AXF5QD61) *Bay Carbon BCI-100HD	Pocographite, Inc. Decatur, TX 76234 Bay Carbon, Inc. Bay City, M 48707
Furnace Power Supply	SCR Power Supply, Model 10- 250	Electronic Measure- ments, Inc. Oceanport, NJ 07757
Excitation Source	300 W Eimac xenon arc lamp at 20 A.	Varian Associates, Eimac Division, San Carlos, CA 94070
Hollow Cathode Lamp		Varian Associates, Eimac Division, San Carlos, CA 94070
Programming/ Timing Unit		Locally constructed(34)
Lenses	2 in dia spherical	
Mirror	6 in spherical	
----- continued		

TABLE 3-continued

Component	Model No.	Company
Atomizer		Locally-constructed described in text
*Wavelength Modulation Function Generator and Torque Motor Driver		Locally-constructed described in text
*Quartz Refractor Plate	Spectrosil, $1_{in} \times 1_{in} \times 1/8_{in}$	
*Torque Motor	Mechanics for Electronics Series R4-077	MFE Corp., Keewadin, Dr., Salem, NH 03079
*Modulation Frequency	80 Hz	
*Integrator	Optically triggered	Locally-constructed, described below
*Optical Transistor		Mounts locally-constructed, described below
*Output DVM	Model 8000A Fluke digital volt meter	
*Recording Oscilloscope	Tektronix Model 549 storage scope with 1A1 dual trace plug-in and an oscilloscope camera	Tektronix, Inc., S. W. Millikan Way, Beaverton, OR 97005

* Indicates additions or changes to original system as studied by Vaughn (34)

TABLE 4
RESULTS OF THE OIL CORRELATION SAMPLE ANALYSIS, CONCENTRATIONS IN ppm($\mu\text{g g}^{-1}$)

Sample	Cu			Meets Criteria ^b	Mo ^c			Meets Criteria ^b	Al			Meets Criteria ^b
	Trimmed ^a Mean	Work	%RSD		Trimmed ^a Mean	Work	%RSD		Trimmed ^a Mean	Work	%RSD	
181	35.85	35.22	16.5	Y	-	-	-	-	13.48	15.62	7	Y
182	31.28	32.35	5.4		-	-	-	-	11.51	12.99	27	
183	6.32	6.26	12.5	Y	-	-	-	-	15.14	13.20	3	Y
184	5.46	4.93	10.7		-	-	-	-	13.14	10.07	15	
193	9.84	9.85	5.1	Y	40.87	41.84	23	Y	-	-	-	-
194	8.40	9.34	4.5		35.90	39.27	10		-	-	-	
195	5.20	4.86	6.1	Y	-	-	-	-	-	-	-	-
196	4.40	3.99	17.8		-	-	-	-	-	-	-	-
197	46.86	47.74	3.6	Y	-	-	-	-	-	-	-	-
198	43.20	48.03	1.9		-	-	-	-	-	-	-	-

^aThis is the mean from 61 laboratories participating in the JOAP

^b(Y) indicates the results meet the criteria for repeatability and accuracy as set forth by JOAP

^cThe values for Mo are AE results. Also, since so few of the labs in JOAP determine Mo, this data had to be obtained by telephone from Pensacola NAS Interservice Oil Analysis office. No data available for 181, 182, 183, 184, 195-198.

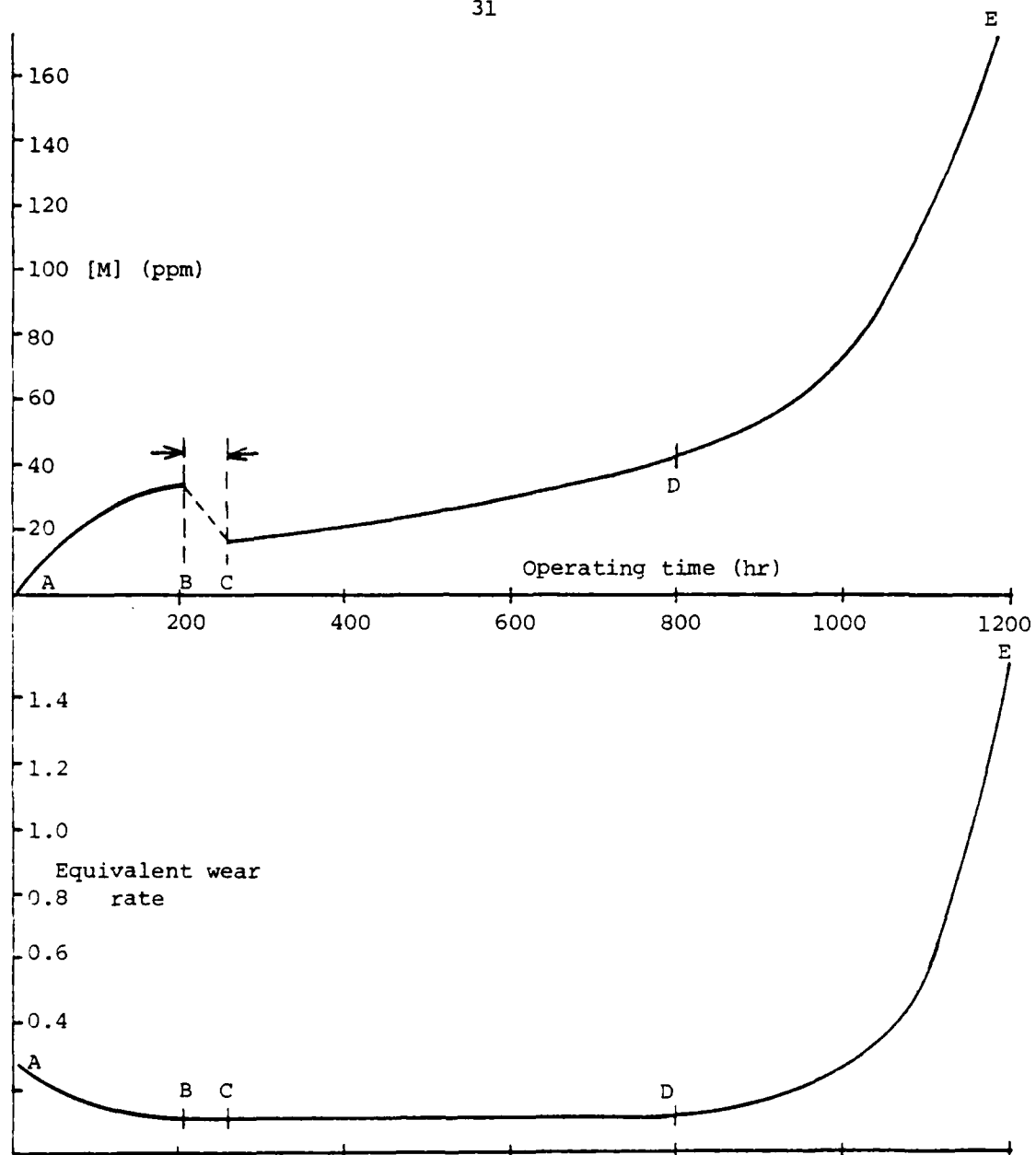
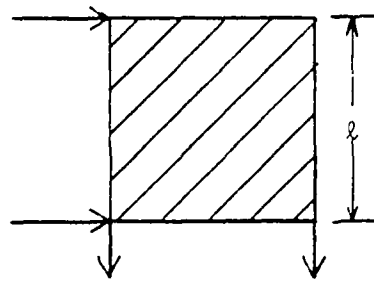
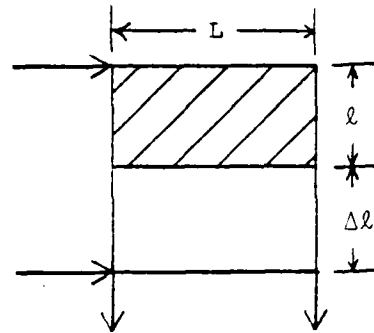


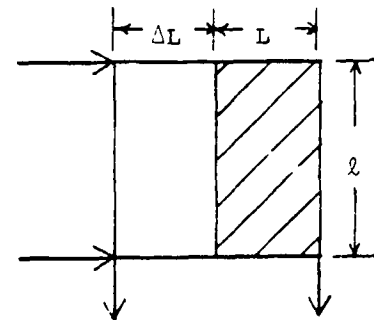
Figure 1: Time relationship of wear metal concentration in lubricating oil (top curve) and the equivalent wear rate of the engine (bottom) derived from the top curve by differentiation



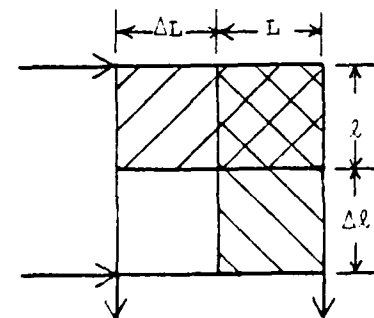
(a) Complete illumination-complete measurement of fluorescence



(b) Incomplete illumination-complete measurement of fluorescence



(c) Complete illumination-incomplete measurement of fluorescence



(d) Incomplete illumination-incomplete measurement of fluorescence

Figure 2: Different illumination and observation geometries in a practical fluorescence set-up.

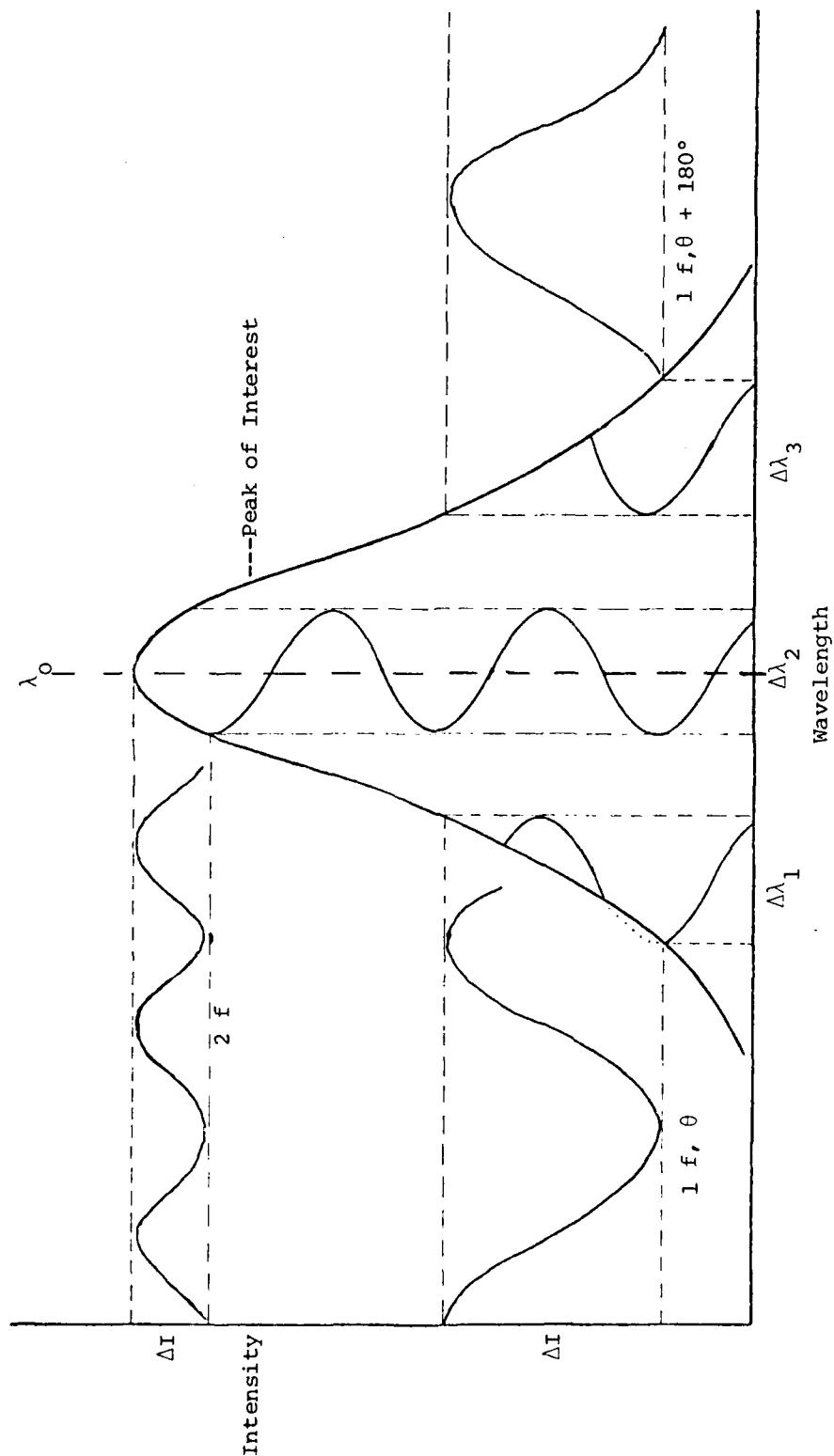


Figure 3: Graphical representation of wavelength modulation; λ_0 is the wavelength of the analyte line of interest. $\Delta\lambda$ represents the wavelength interval over which modulation occurs. f is the frequency of the modulation signal, represented by the vertical sine waves. By varying the position of the modulation interval in relation to λ_0 , the output signal represented by the horizontal sine waves can be changed in amplitude, frequency and phase angle (θ).

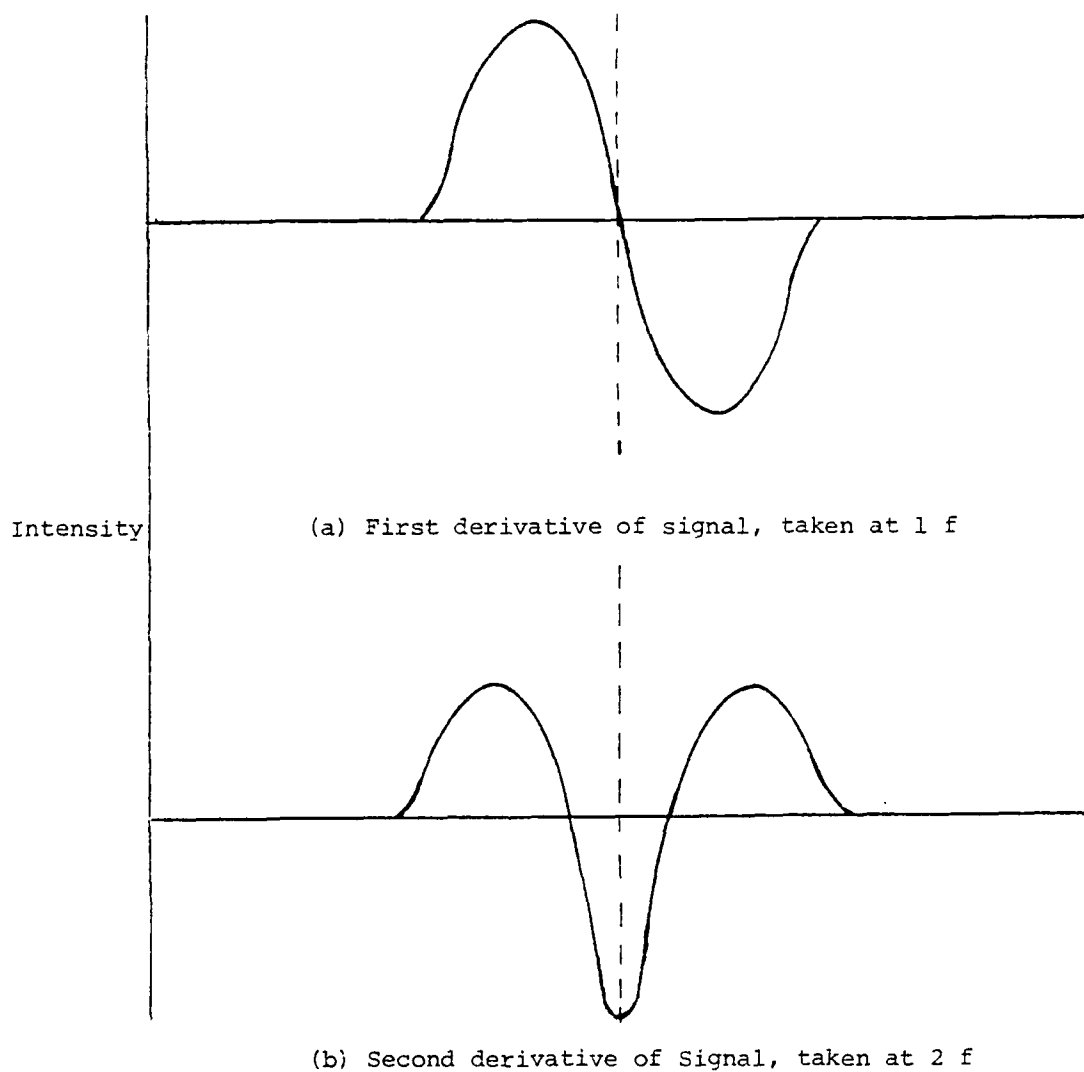


Figure 4: Typical waveforms at $1 f$ and $2 f$, where f is the frequency of the modulation signal. The derivatives are only approximate, since $\Delta\lambda$ is not infinitesimally small.

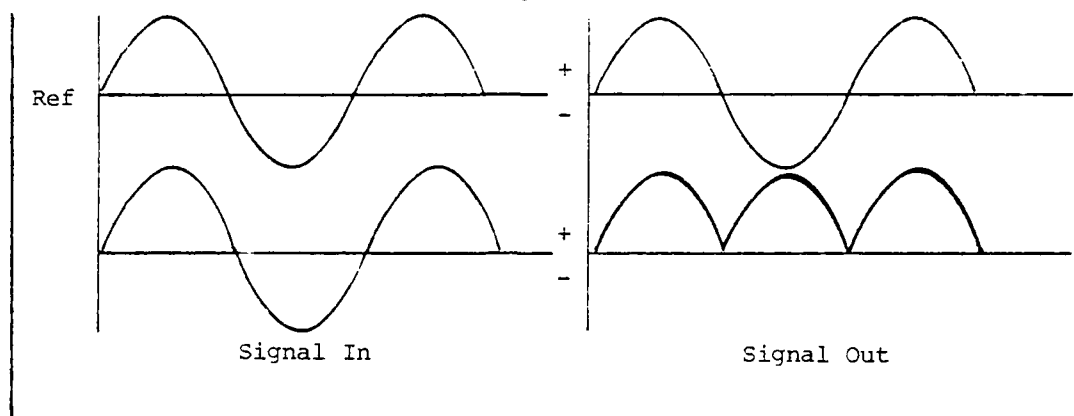


Figure 5: Signal of interest is in phase with the reference signal (i.e. $\theta = 0^\circ$) and the output signal is at the maximum value: $E_{DC \text{ out}} = \frac{2}{\pi} E_{\text{max}}$

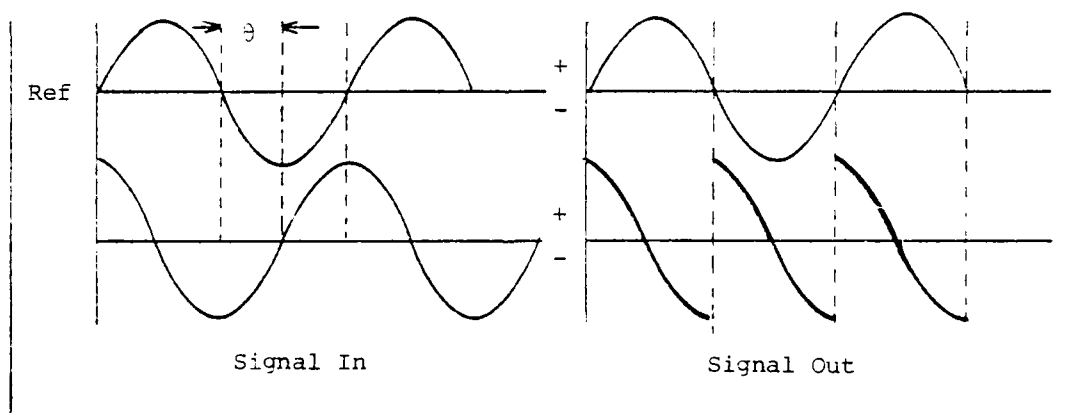


Figure 6: Signal of interest is 90° out of phase with reference (i.e. $\theta = 90^\circ$) with a resulting net DC output of zero

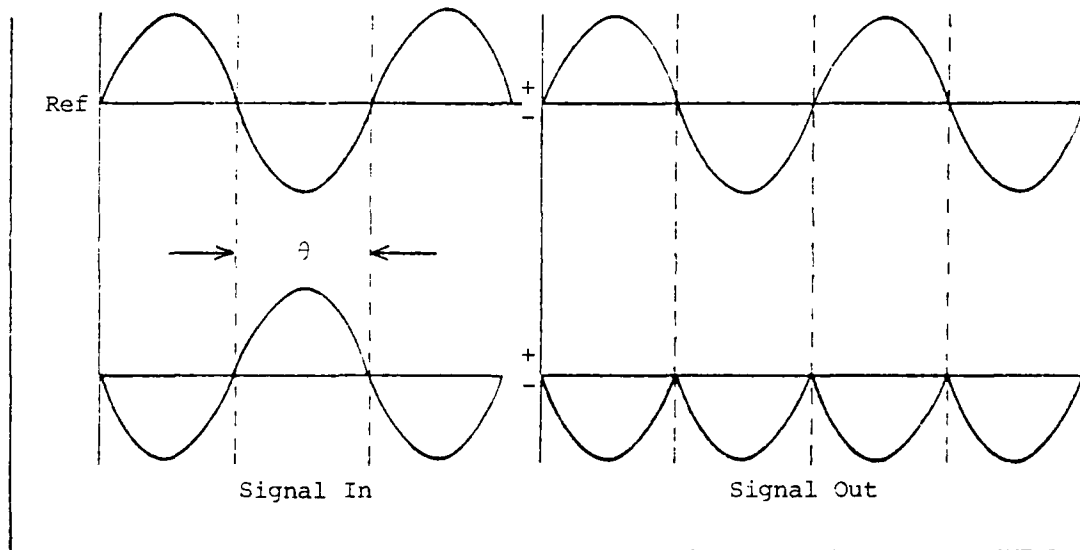


Figure 7: Signal input is 180° out of phase with the reference signal. The output is the same as in the $\theta = 0^\circ$ case, except that the polarity is negative: $E_{DC} = -\frac{2}{\pi} E_{max}$

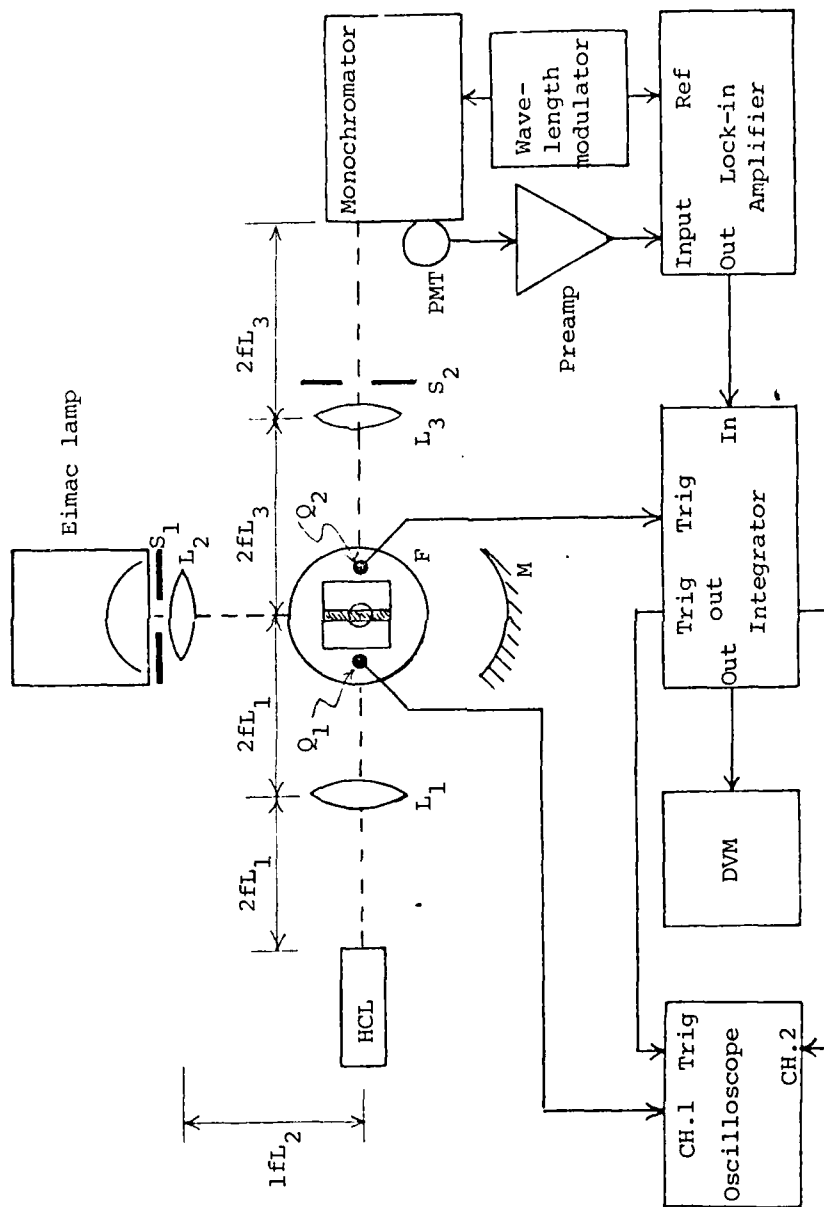


Figure 8: Schematic of experimental system. Lenses L_1 , L_2 , L_3 focus the source and the measurement beams. Focal lengths of the lenses are represented by f . Q_1 is an optical transistor used for temperature measurements. Q_2 is a second optical transistor used to trigger the integrator. F is the furnace-burner combination. M is a 6 in spherical mirror. S_1 and S_2 are 1 cm light stops.

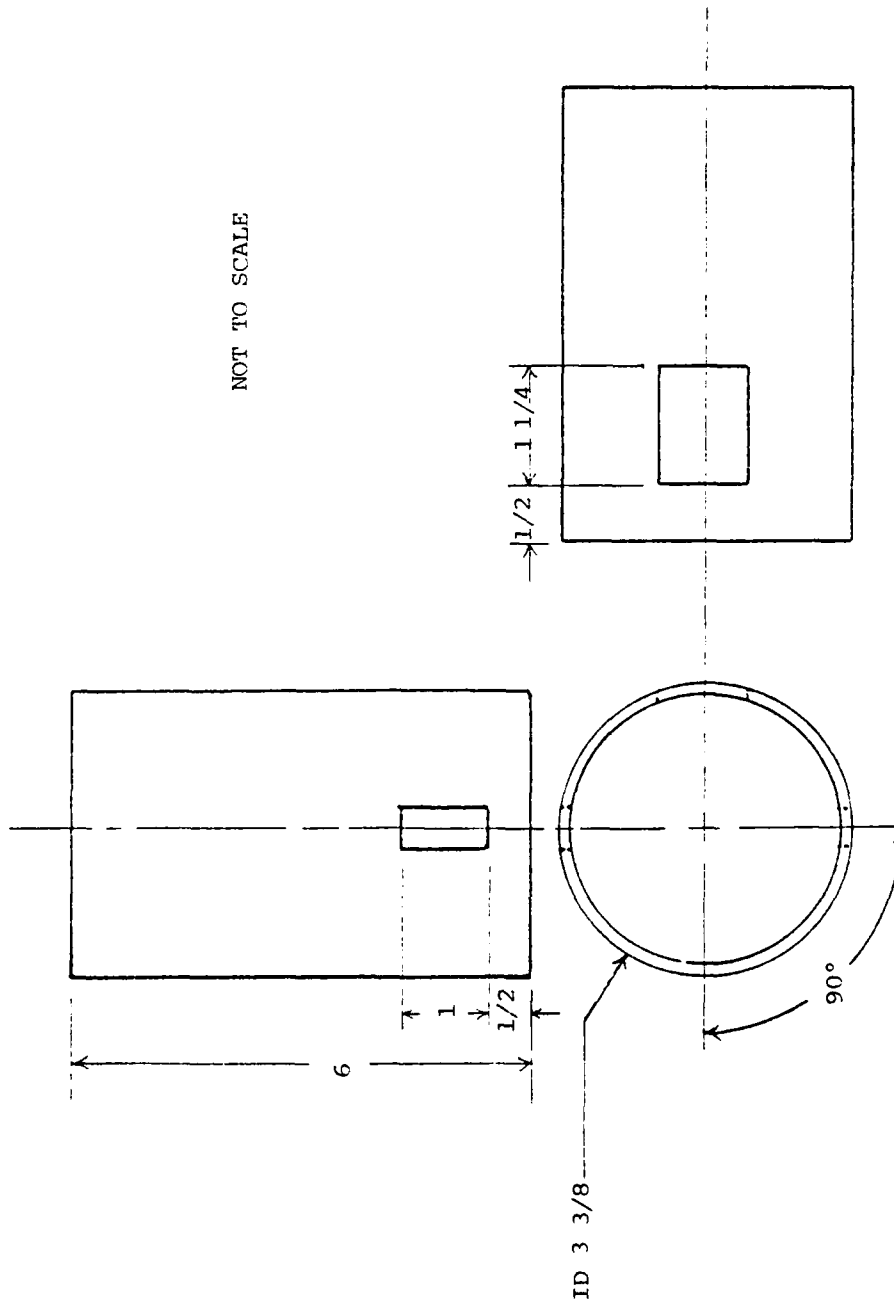


Figure 9: Light trap for burner head. Trap was constructed from aluminum stock. Final turned thickness was 1/4". Entire trap was painted flat black. The trap was fitted around circular burner head when in use. All dimensions in inches

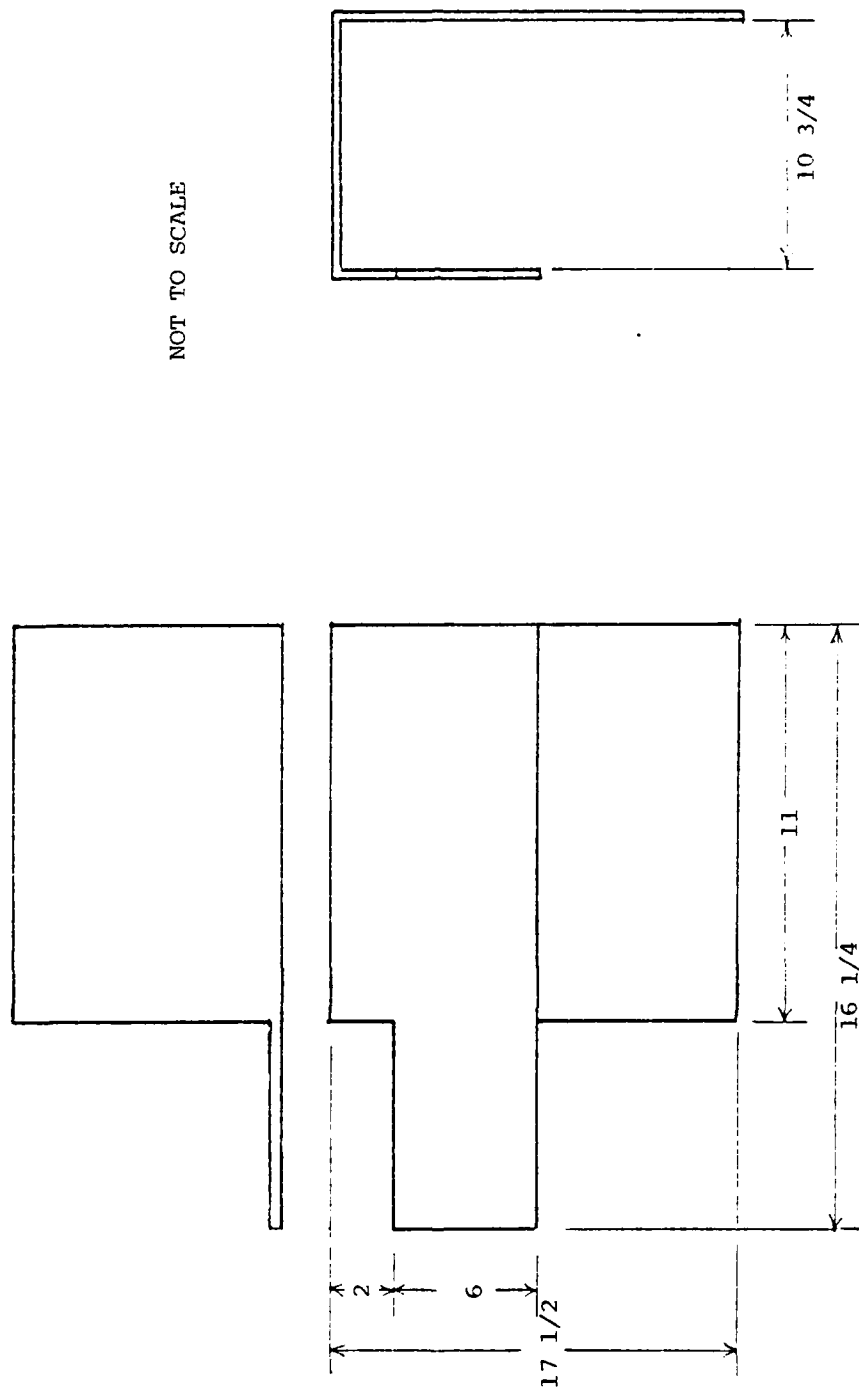


Figure 10: Light trap for focusing lenses and monochromator slits. Trap was constructed of sheet steel and painted flat black. This trap was placed between burner and monochromator to block stray environmental light. All dimensions in inches.

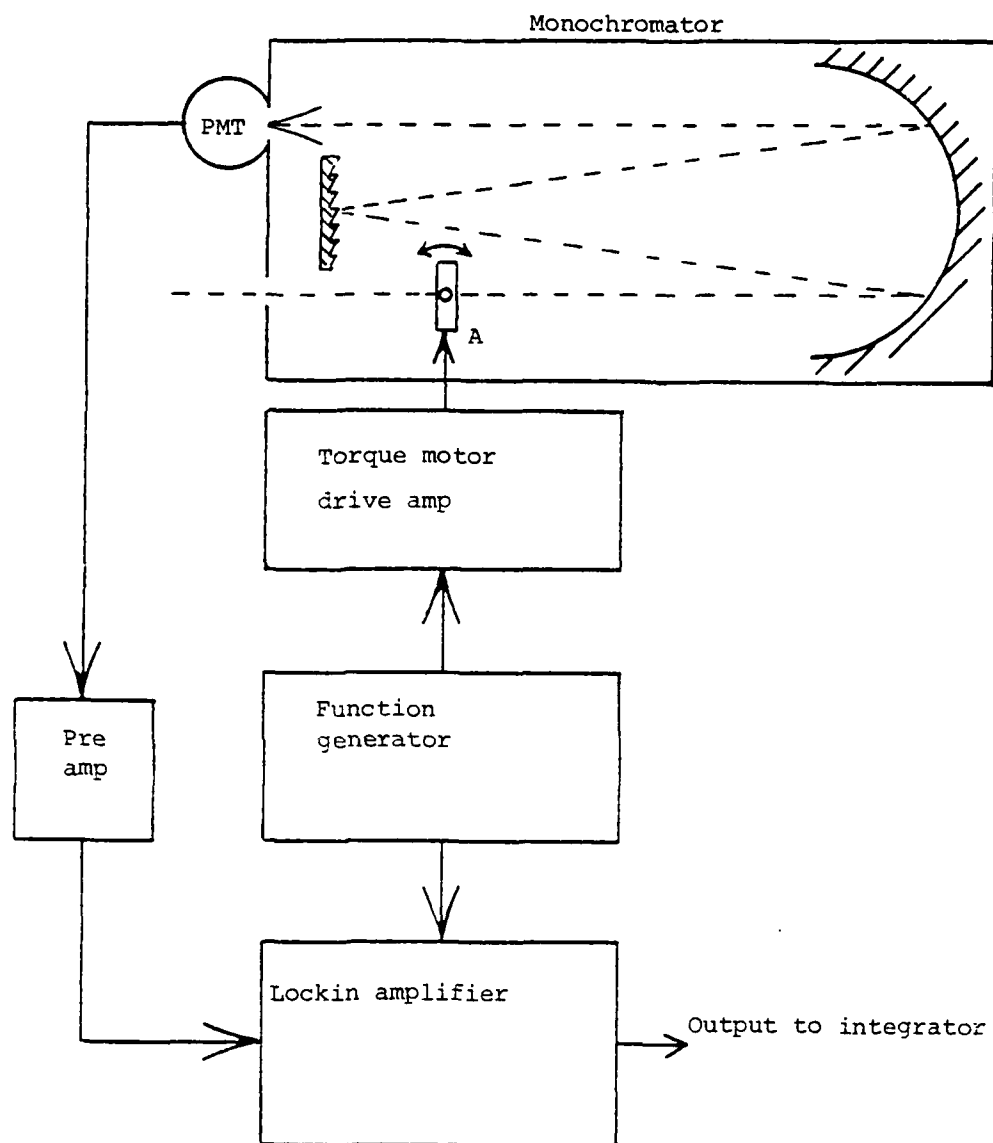


Figure 11: Schematic depicting the geometry and flow diagram for the quartz refractor plate and torque motor (A) and the oscillator and driver circuits. (See Appendix A for more circuit information.)

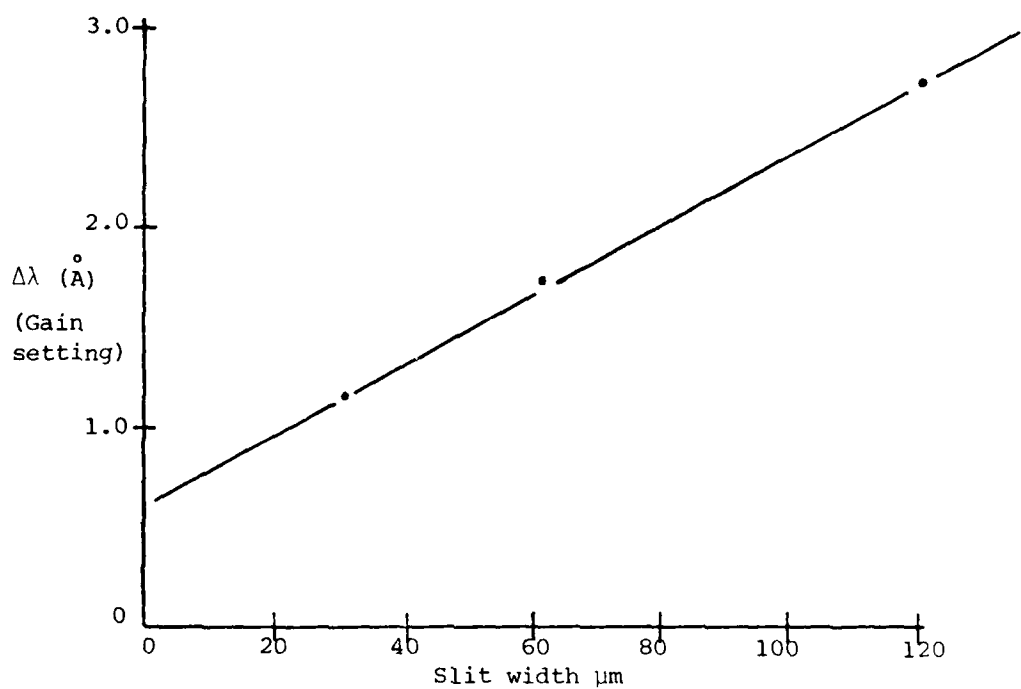
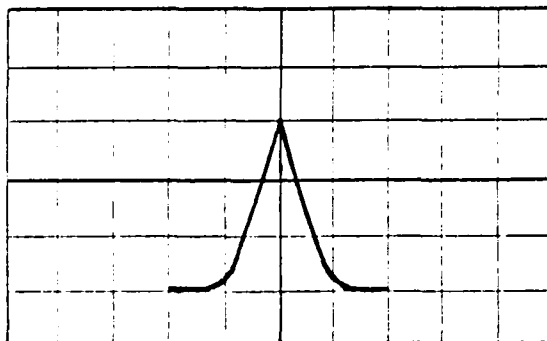
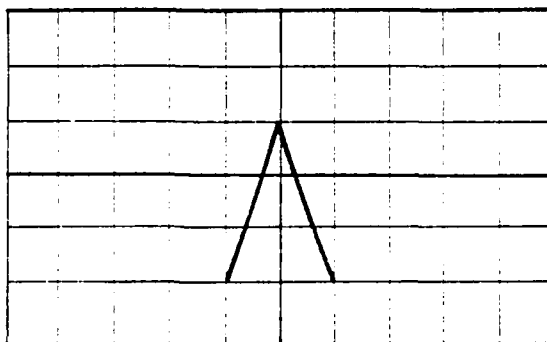


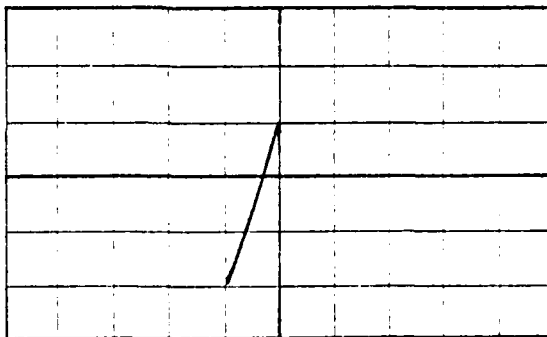
Figure 12: Calibration curve for wavelength modulation system. Plot depicts the optimum gain setting versus slit width. The value is determined by observing peak shape on an oscilloscope while varying the $\Delta\lambda$, slit width constant. When the peak shape is that of Figure 13 (b), i.e. $\Delta\lambda = 2$ s, signal conditions are optimum



(a) $\Delta\lambda \gg 2S$, S = Spectral bandpass



(b) $\Delta\lambda = 2S$; $2f$ signal max.; $1f$ signal min.



(c) $\Delta\lambda = D$; $2f$ signal min.; $1f$ signal max.

Figure 13: Estimation of $\Delta\lambda$ and optimization of signal. These are typical oscilloscope traces of an atomic emission (HCL) line being wavelength modulated. If $\Delta\lambda$ is large as in (a), the background appears. At the optimum conditions for a $2f$ signal (b) only the peak appears. At optimum $1f$ conditions, only half the peak is visible

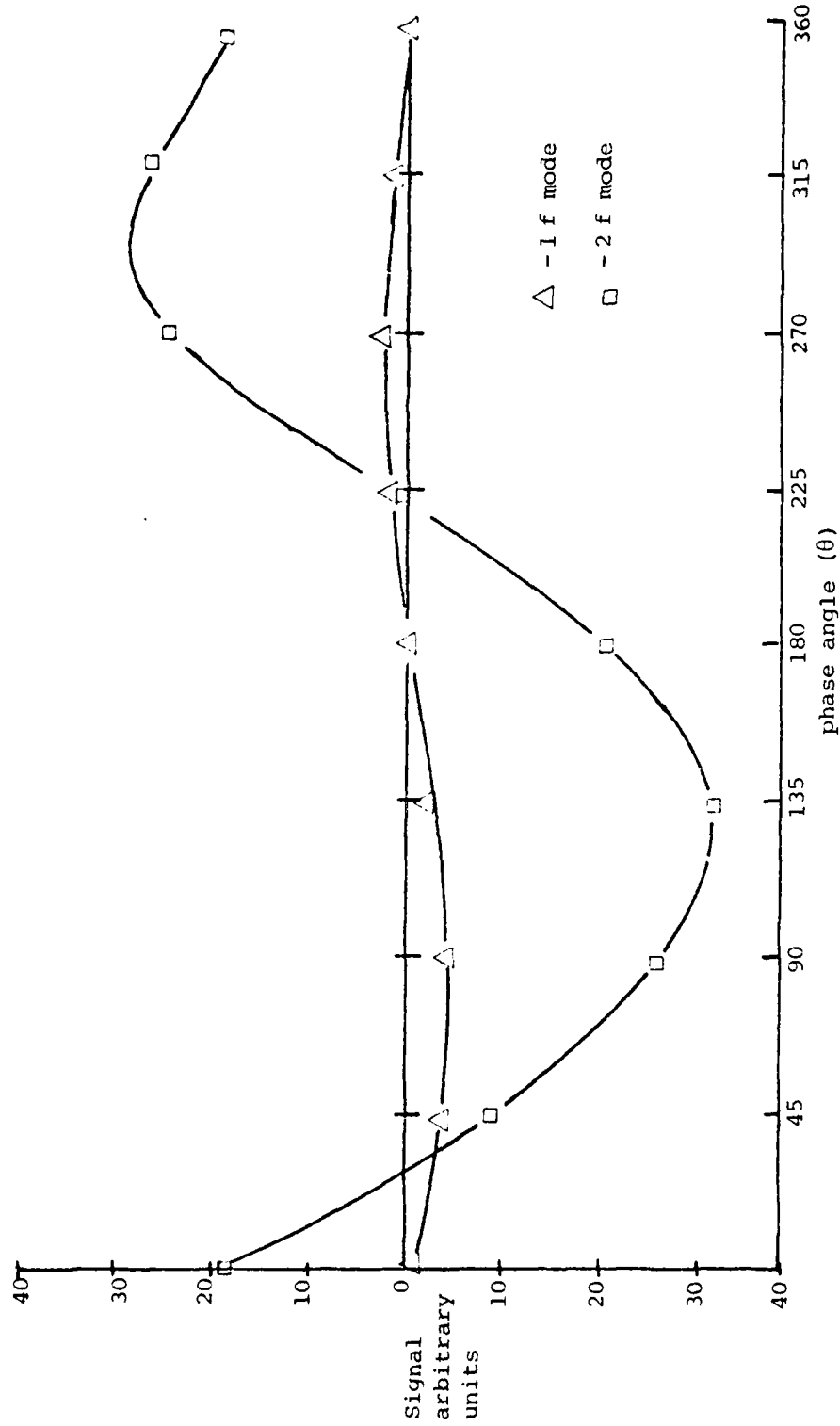


Figure 14: Signal versus phase angle. By varying the phase angle from 0° to 360° , the effect is the same as scanning the wavelength all the way across the $\Delta\lambda$ interval and back (see Figure 3). This plot is the result of such a scan, both at $1f$ and $2f$ (where f = modulation frequency) when $\Delta\lambda$ is centered on λ_0 . As expected, the $2f$ signal is much larger.

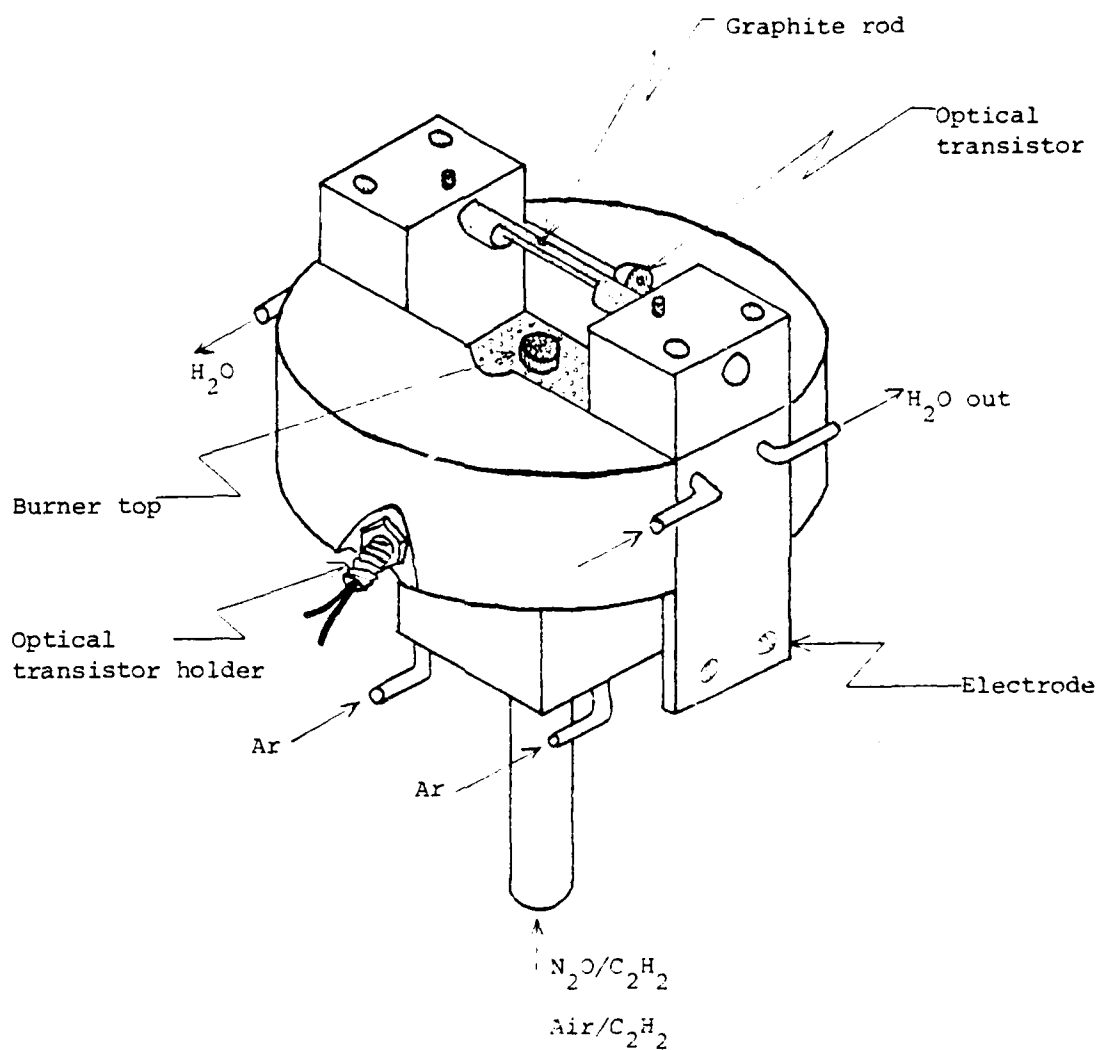


Figure 15: Depiction of the combination graphite filament furnace and flame atomizer showing the location of the optical transistors

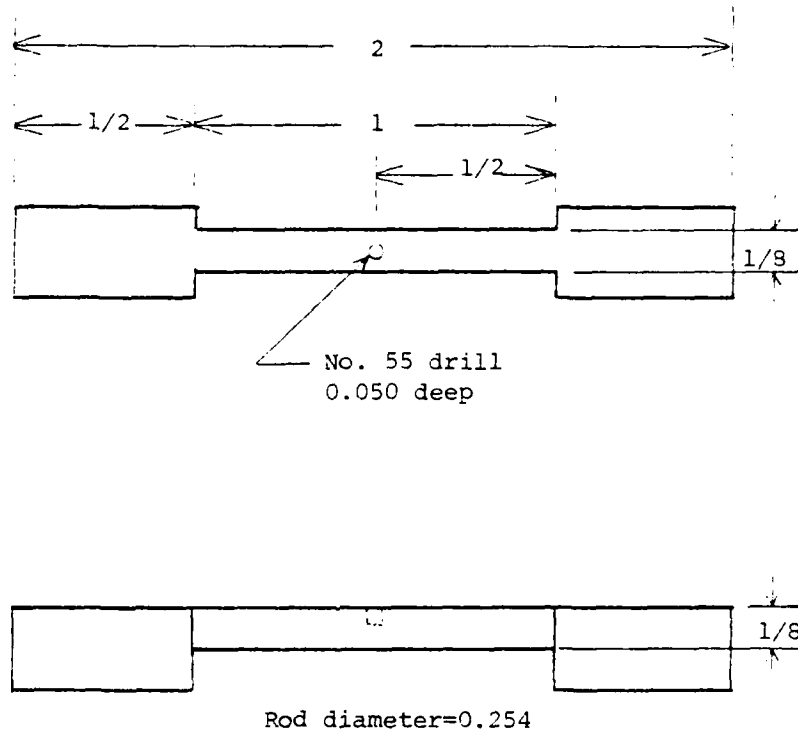
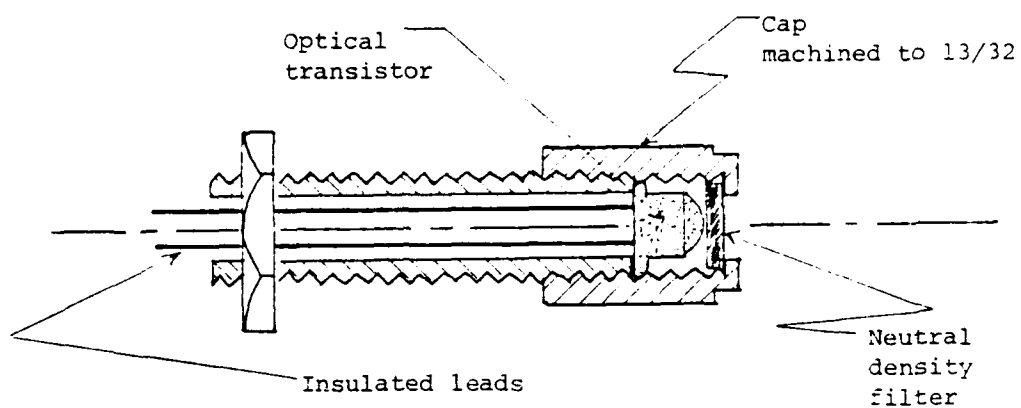
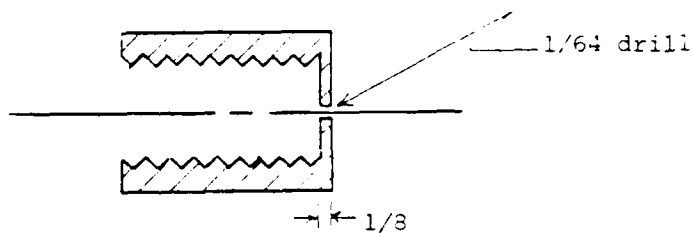


Figure 16: Graphite filament design. Materials as described in Table 3. All dimensions in inches

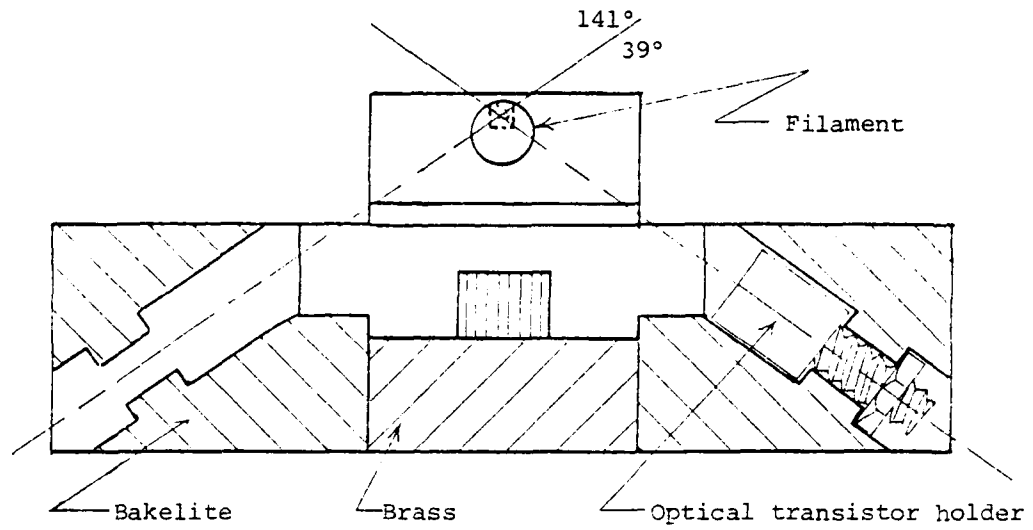


(a) Transistor holder with low temperature and trigger cap.
 Tube is 1/4 in. stainless steel or brass Swagelok fitting.

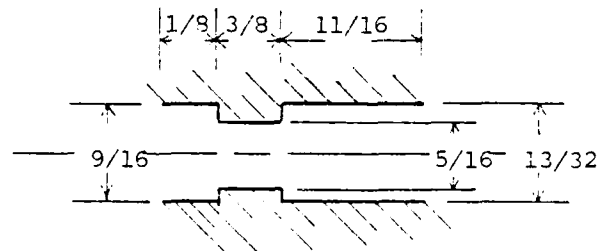


(b) This drawing depicts the cap used for the high temperature measurements. No filters were required.

Figure 17: Design of optical transistor holder (designed and constructed by the author). All dimensions in inches



- (a) A cutaway view of the burner head depicting the mounting passages for the optical transistor holders and their alignment. Holder is in place on right.



- (b) Actual dimensions of the drilled passages.

Figure 13: Design of the optical transistor mounts. (Designed and constructed by the author). All dimensions in inches

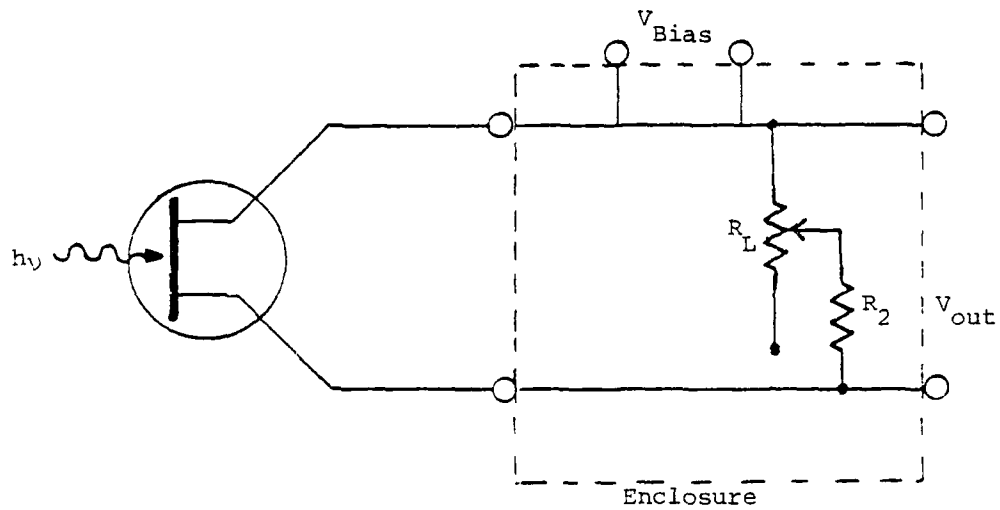


Figure 19: Biasing circuit for the optical transistor for filament temperature measurements. V_{Bias} was $+15V_{dc}$. R_L was a ten-turn potentiometer which was used to vary the temperature response range of the transistor. R_2 was externally mounted for ease of fixing ranges. Normally $R_2 = 0$.

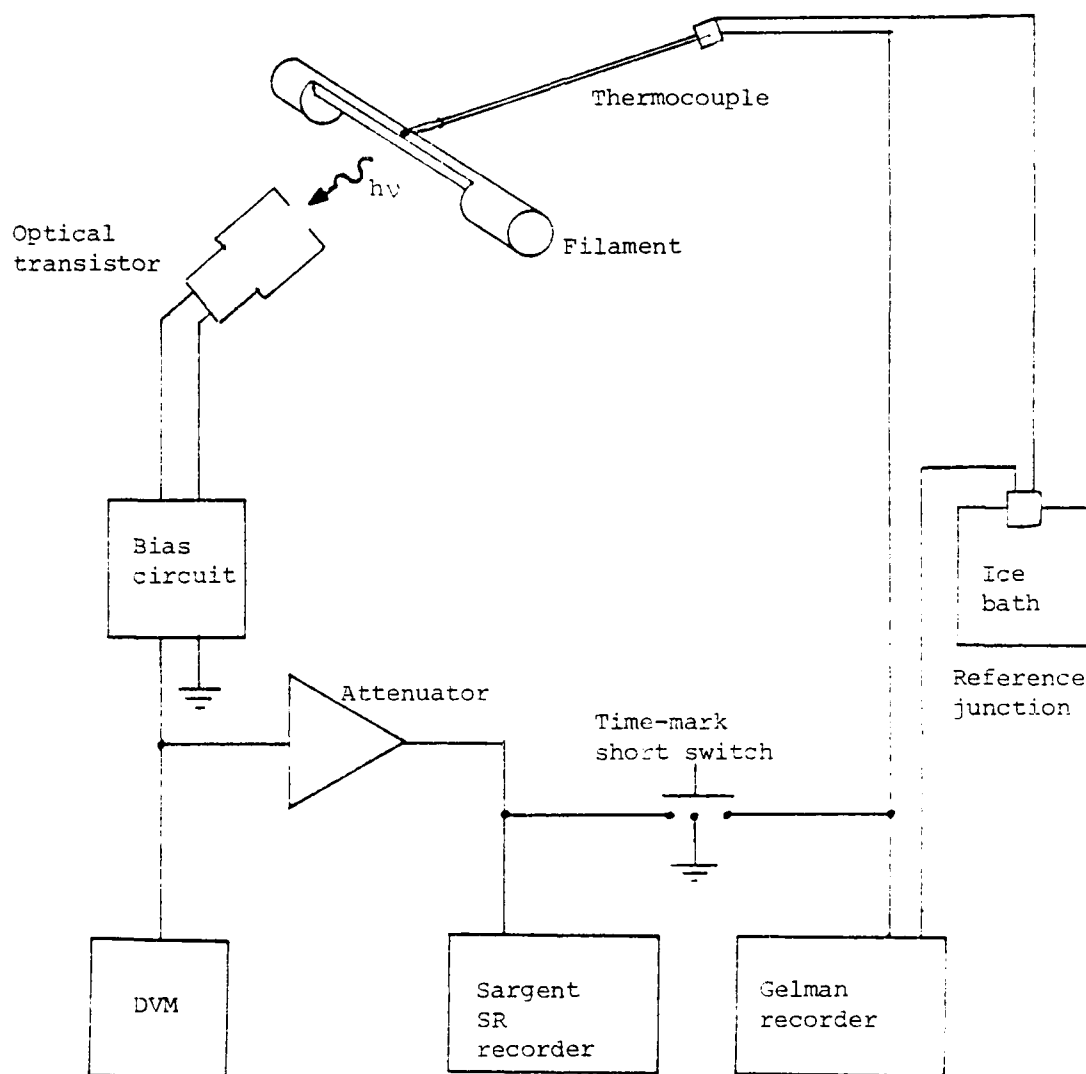


Figure 20: Block diagram representing the scheme for the optical transistor temperature calibration measurements. The attenuator was used to match transistor output with recorder scale. Short switch was used to synch the recording strips

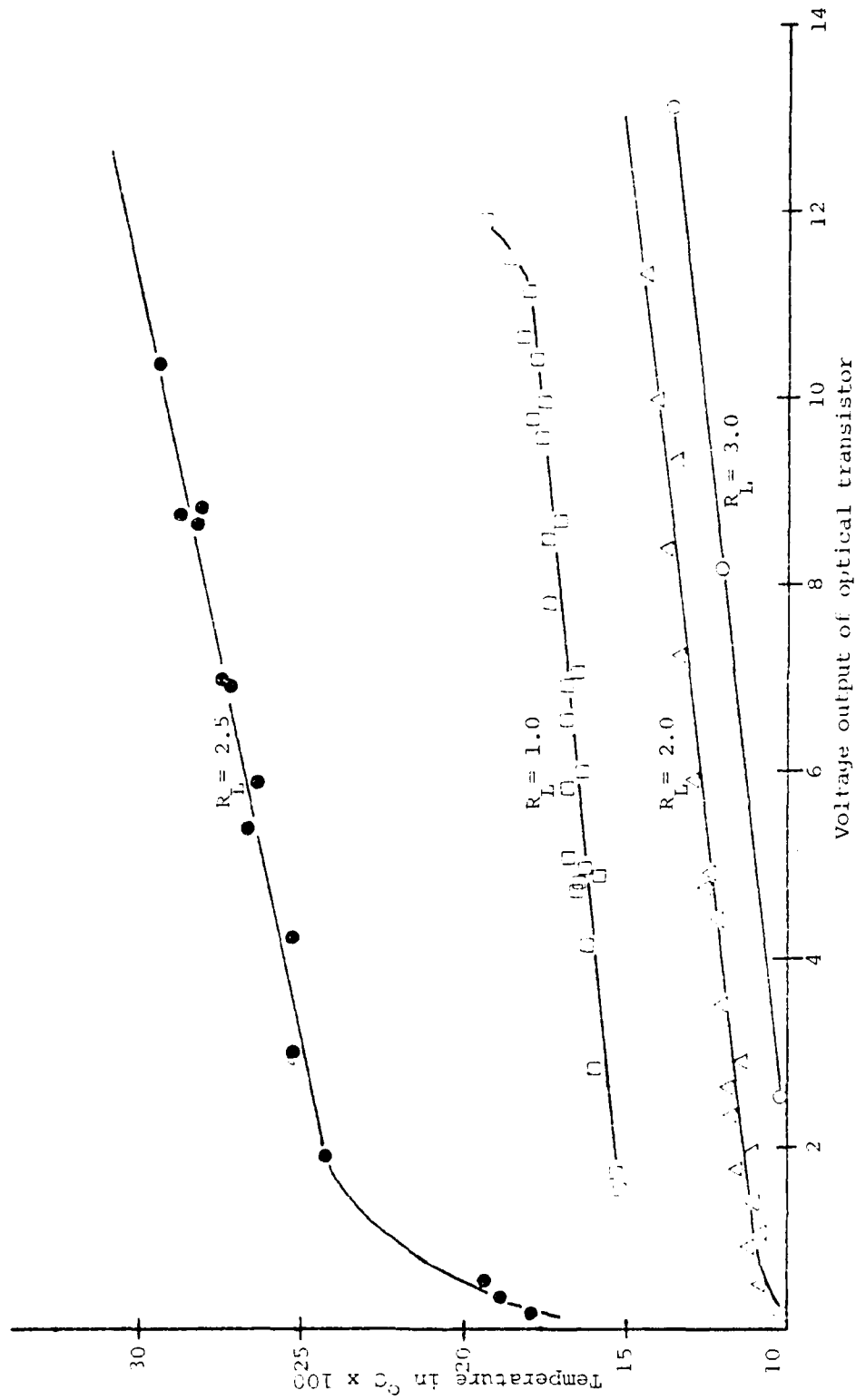


Figure 21: Temperature calibration curves for the optical transistor. Top curve measured with the high temperature cap (see Figure 7 (b)), the other three with the low temperature cap. R_L values in the bias circuit were as noted.

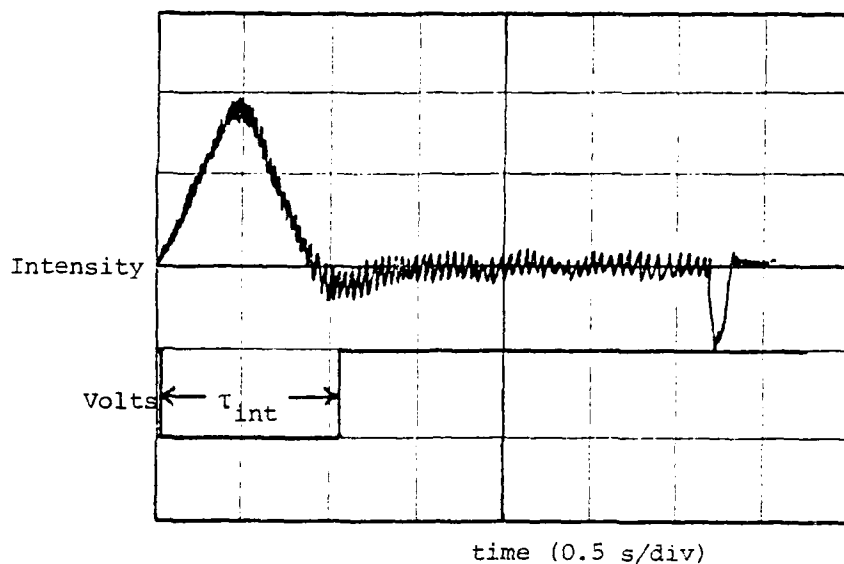


Figure 22: Typical oscilloscope trace for a Cu signal for setting the integration time (τ_{int}). Upper trace is a Cu fluorescence signal.

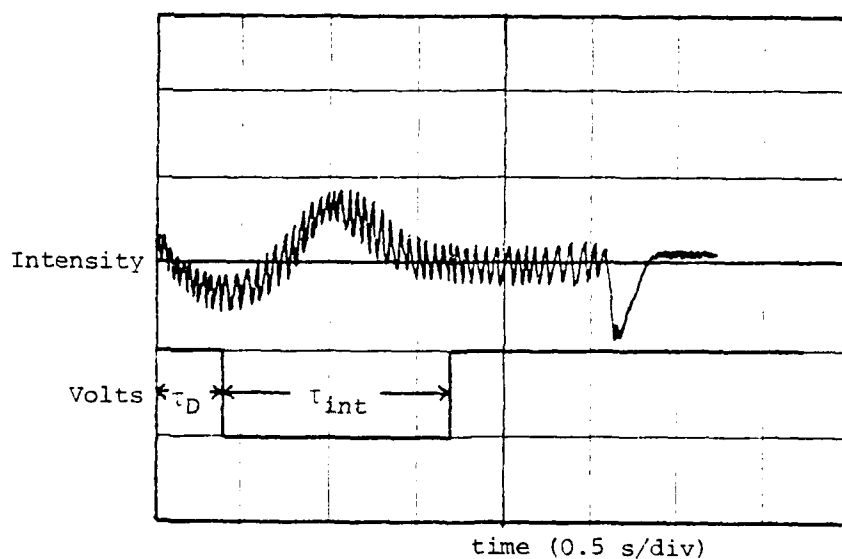


Figure 23: A second example of the setting of τ_{int} and the delay time (τ_D). 50 ppm Mo trace at top. Notice negative signal at the beginning due to the out of phase N_2O/C_2H_2 noise. Drop at the end due to flame pop when extinguishing.

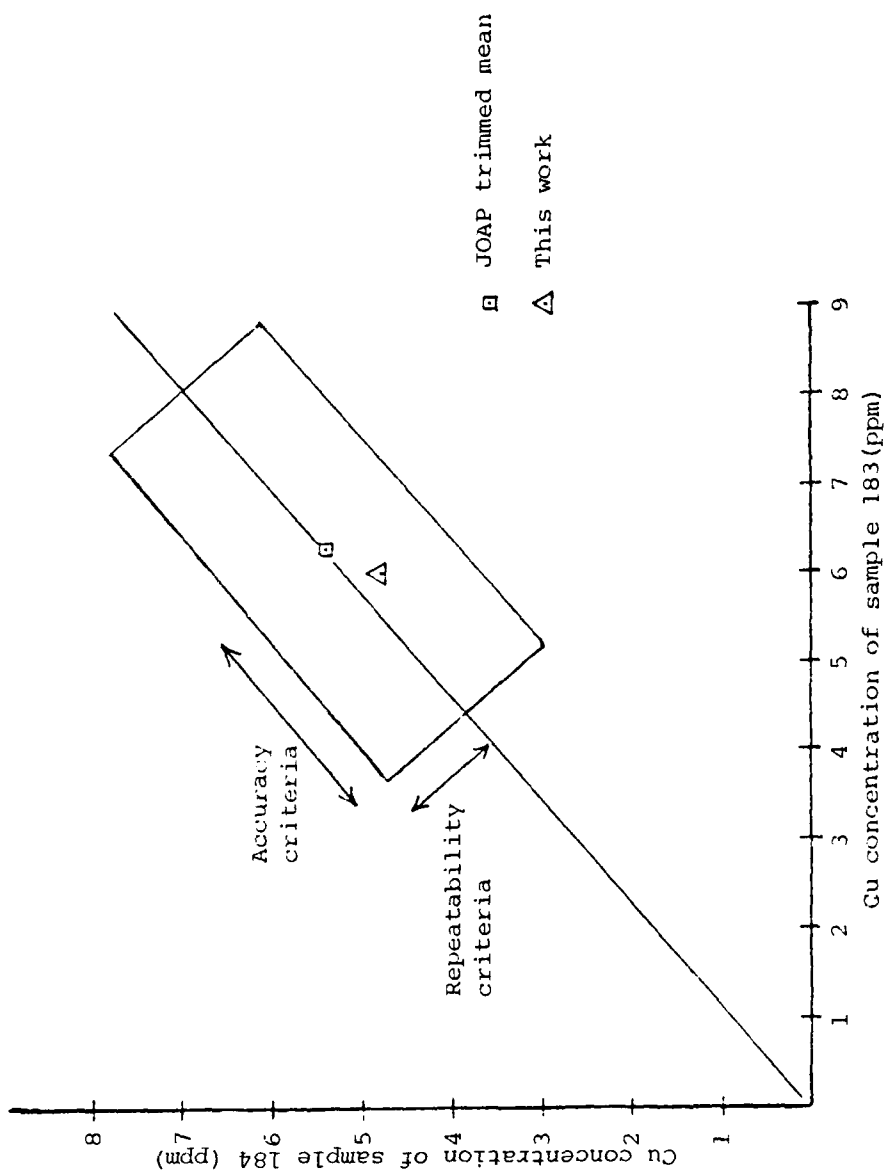


Figure 24: A plot of JOAP accuracy and repeatability criteria for the Cu concentration of JOAP correlation sample No. 184 and 183. The criteria are established by JOAP and published monthly. The criteria and the trimmed mean are based on the analysis of the same sample by 61 laboratories. Note that the value determined in this work falls within acceptable area

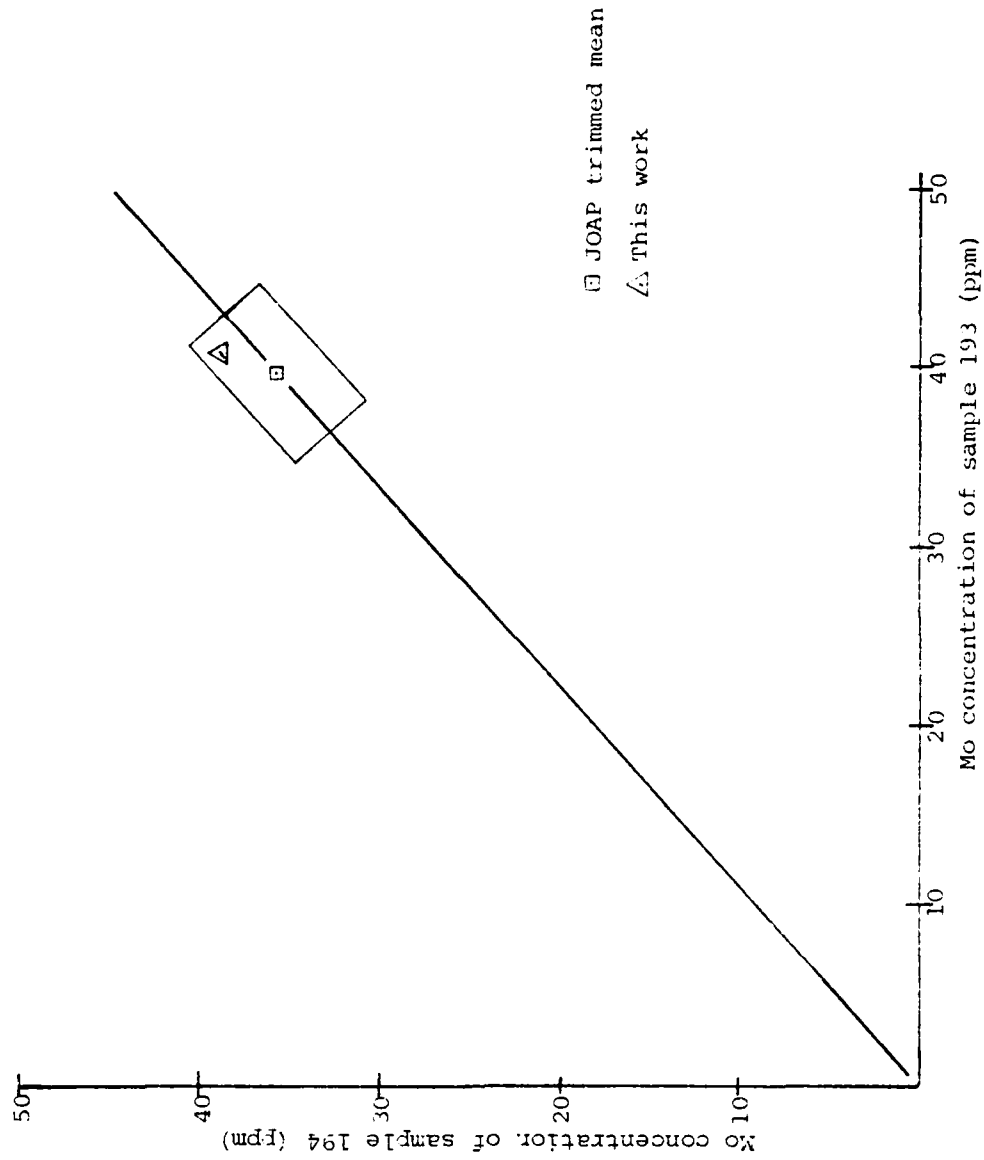


Figure 25: A correlation plot of Mo concentration for JOAP correlation samples No. 193 and 194, with the determination from this work

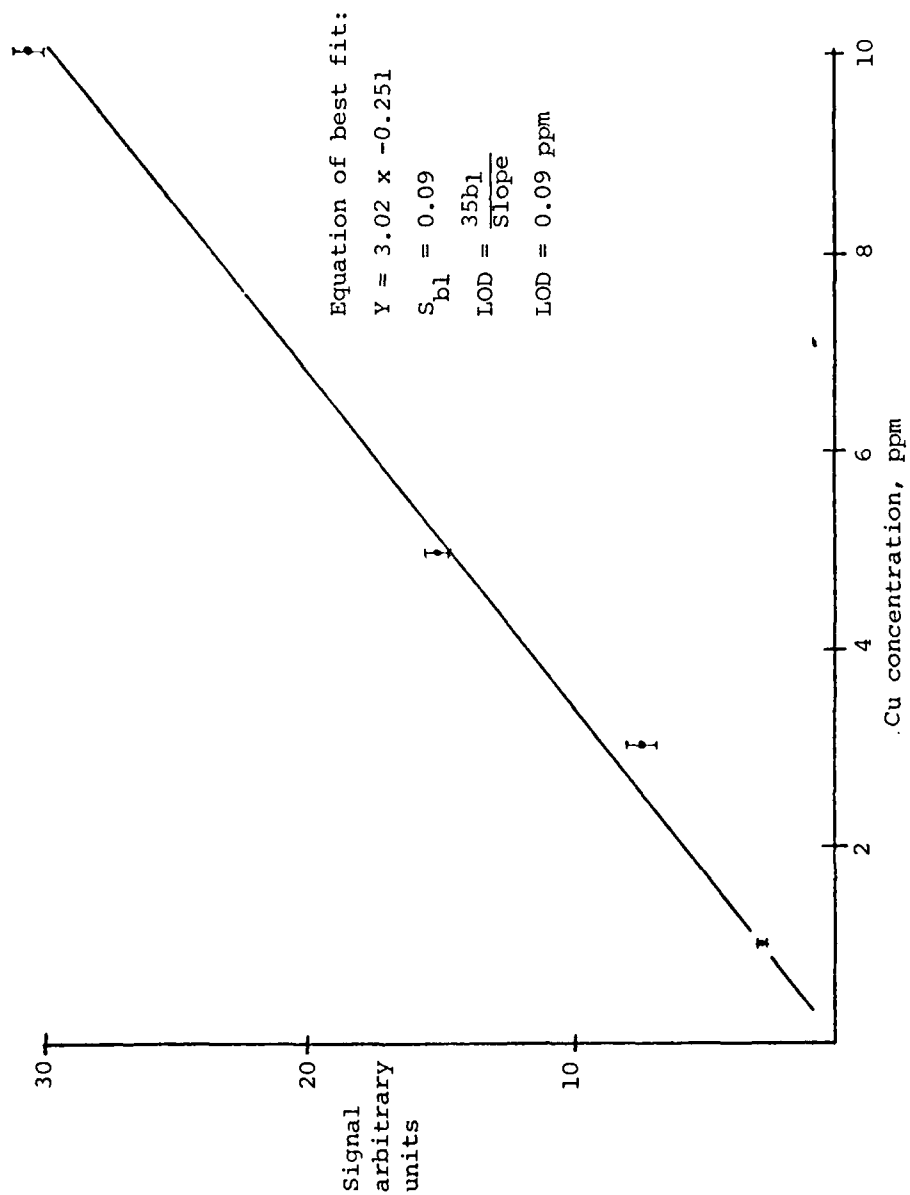


Figure 26: Cu calibration curve from data for SOAP oil standards. All run on a single filament. Equation of best fit and LOD calculations presented. Correlation coefficient is 0.9979

CHAPTER VIII CONCLUSIONS AND FUTURE WORK

The addition of wavelength modulation and optically-triggered integration offered a definite improvement over the system as studied by Vaughn (34). The % RSD values were much lower than in VAUGHN's work, ranging from 2-30% at the higher temperatures ($> 2400^{\circ}\text{C}$) and 2-6% at 2000°C . The system was successful in determining Cu, Mo and Al in real jet lubricating oils, with LOD values of 0.09 ppm, 0.4 ppm and < 1 ppm, respectively.

The major source of uncertainty was the rapid deterioration of the filament, agreeing with the conclusions of Vaughn (34). Future work should concentrate on this problem initially. Possible solutions include pyrolysis of the filament, changes in filament shape and design and the use of a more sophisticated optical-transistor driven temperature control system.

Once the filament has been stabilized, study should include further automation using microprocessors, and multielement adaptation with a direct reader.

APPENDIX A
WAVELENGTH MODULATOR SCHEMATIC

The wavelength modulator circuit as presented in Figure 27 consists of only three major components, an oscillator, a buffer amplifier and a power amplifier to drive the torque motor.

The oscillator is an 8038 astable multifribrator set up for 80 Hz. This IC has both a sine and a square wave output. The sine wave is used to drive the torque motor. The square wave is used to reference the lock-in amplifier and is attenuated with a voltage divider to 1-2V peak to peak.

A 747 operational amp (a dual 741) is used to buffer both the outputs.

The power amp is an SI-1020G and the gain is adjusted via a 10kΩ pot.

Not shown is the 50V power supply required by the SI-1020G; however it is simply a transformer, a full wave bridge rectifier and nipple capacitor.

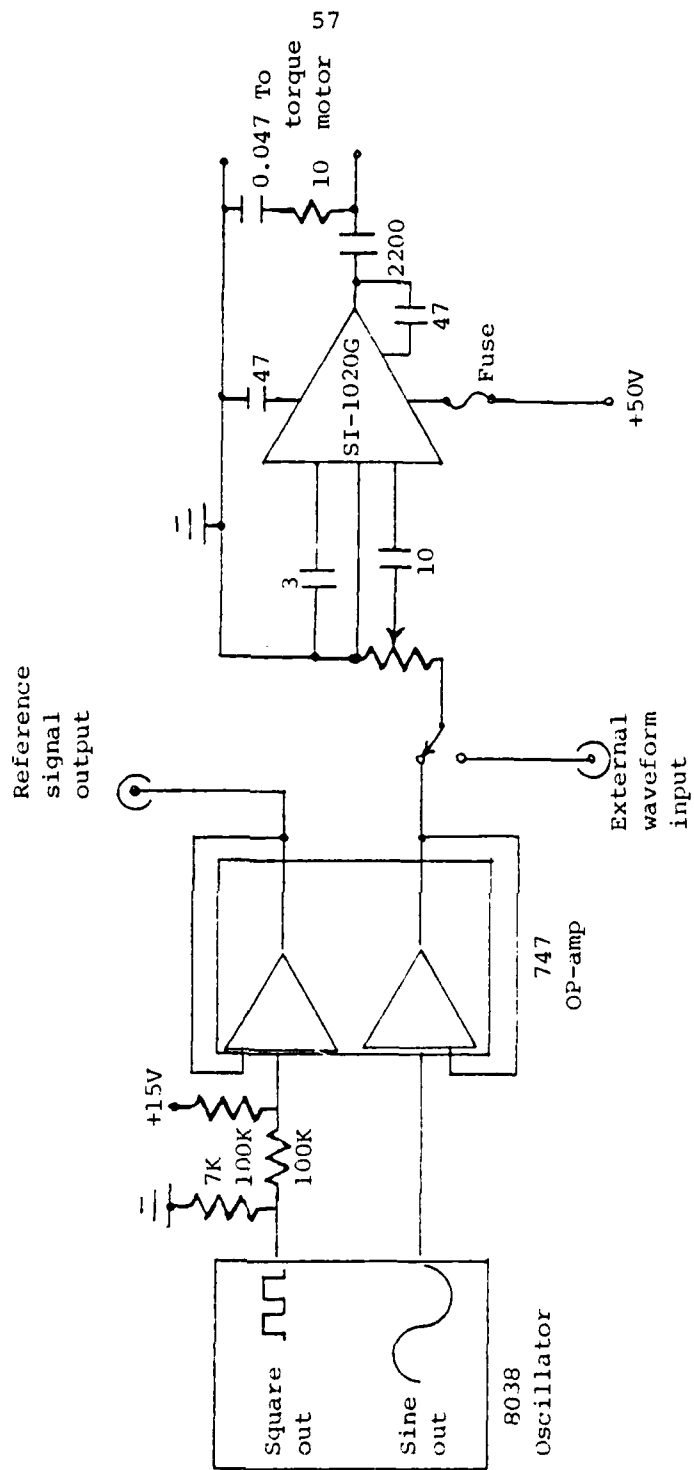


Figure 27: Wavelength modulator circuit. All resistors in ohms, capacitors, in μF

APPENDIX B
OPTICALLY-TRIGGERED GATED INTEGRATOR SCHEMATIC

In this schematic, the integrator has been divided into three sections:

- 1) Triggering circuit, Figure 28,
- 2) Gate control circuit, Figure 29,
- 3) Signal integration circuit, Figure 30.

These are discussed separately below.

The trigger circuit consists of an optical transistor Q_1 which is biased so that light striking the transistor will create a voltage drop which will cause OAl to give a full positive output. This provides the triggering pulse for the gating circuit when S_1 is in the internal position. OAl is in a voltage comparator configuration, and the threshold voltage may be adjusted by R_1 , the temperature potentiometer. Capacitor C_1 AC couples the pulse to the gate circuit, to provide a fast spike which is required to trigger the IC's. Diode D_2 prevents a negative spike occurring when the pulse shuts off, as this would re-trigger the gate. The trigger circuit also has a manual trigger which simply puts +12 volts directly to the gate circuit; AC coupled by C_1 . A trigger monitor is also provided, which is normally used as an oscilloscope trigger.

The gating control circuit consists of three CMOS IC's set up for monostable oscillator operation and one JFET Quad bilateral switch. IC1 controls the delay time through an adjustable RC. IC2 is triggered

by the IC1 output dropping to zero after the selected delay time is over. IC2 then closes one of the switches in IC4 to allow the input signal to the integrator circuit. The gate remains open until the selected RC time is over. IC3 is a reset timer which closes another switch in IC4 after 15 sec. to discharge the integration capacitor. A manual reset is provided which supplies +12 volts to the master reset pins of IC1, IC2 and IC3.

Q_2 is a transistor set up as a voltage follower to provide power for LED normally plugged into the gate monitor.

The integrator circuit includes OA2, which is simply a gain amplifier, with adjustable gain from 0.001X to 10X. When the gate is open, the amplified signal passes to OA₃ which is the integrator. Three integration times are available through a RC selection switch. This integration time is independent of the gate time. OA4 is simply an inverting amplifier, used only if an inverted output is desired.

Not shown is the 12 volt power supply and the many isolation capacitors and trimming circuits.

The following is a list of components:

OA1, OA4	741
OA2	AD40J
OA3	AD40K
IC1, IC2, IC3	CD4047
IC4	LS13202
Q_1	TIL67-T1202
Q_2	2N2222
Diodes	1N914

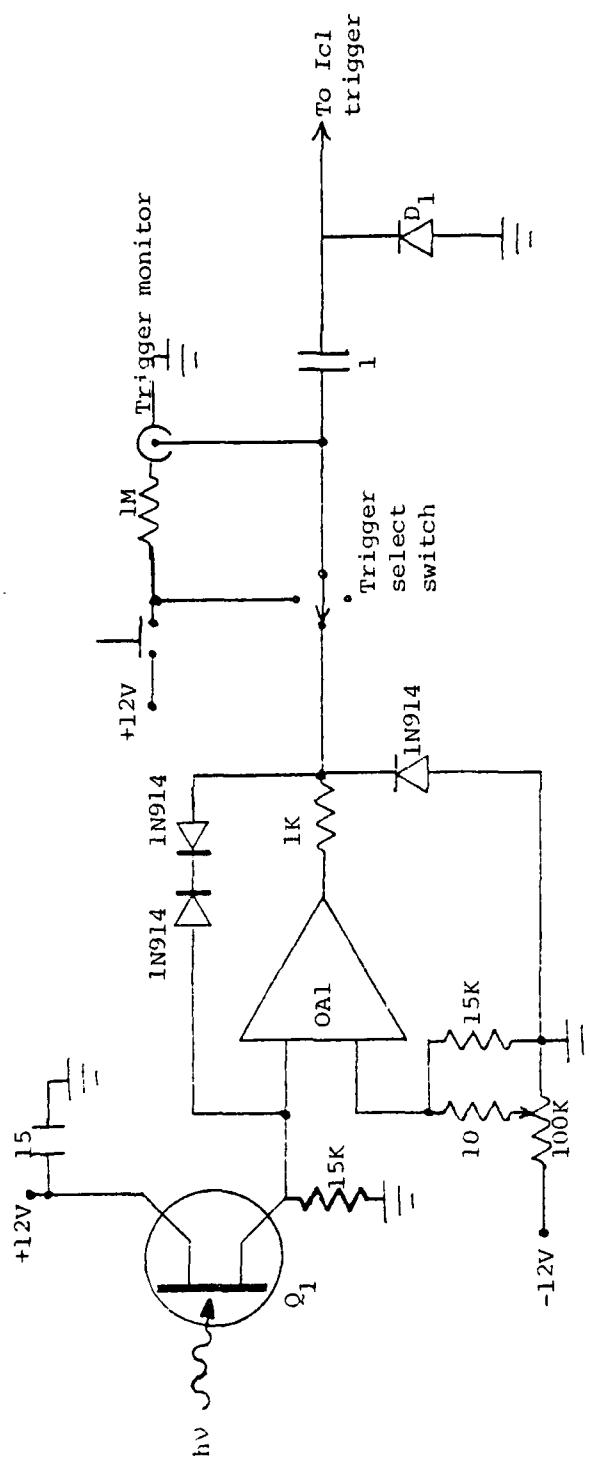


Figure 28: Gated integrator trigger circuit. All resistors in ohms, capacitors in μF

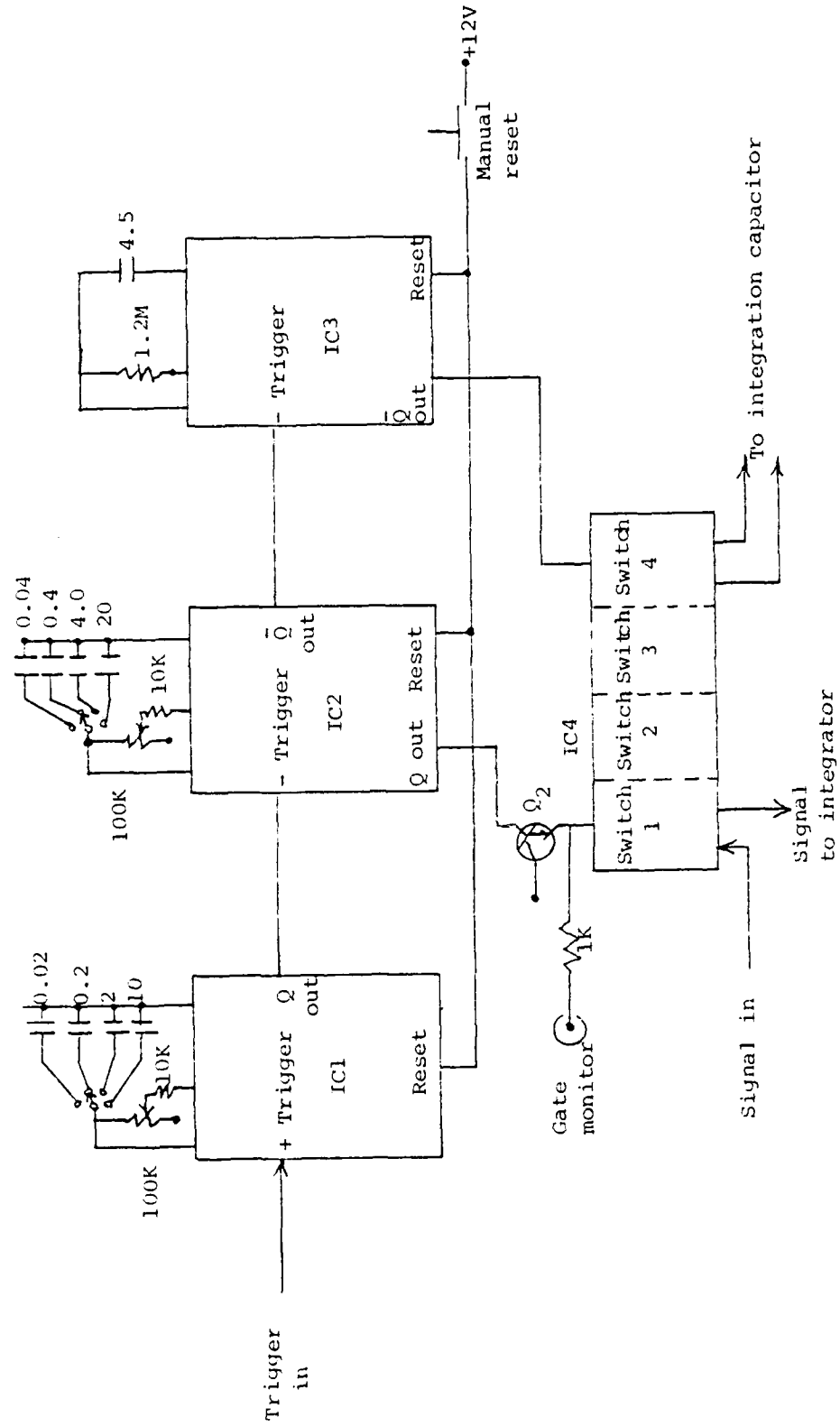


Figure 29: Gated integrator gate control circuit. All resistors in ohms, all capacitors in μF

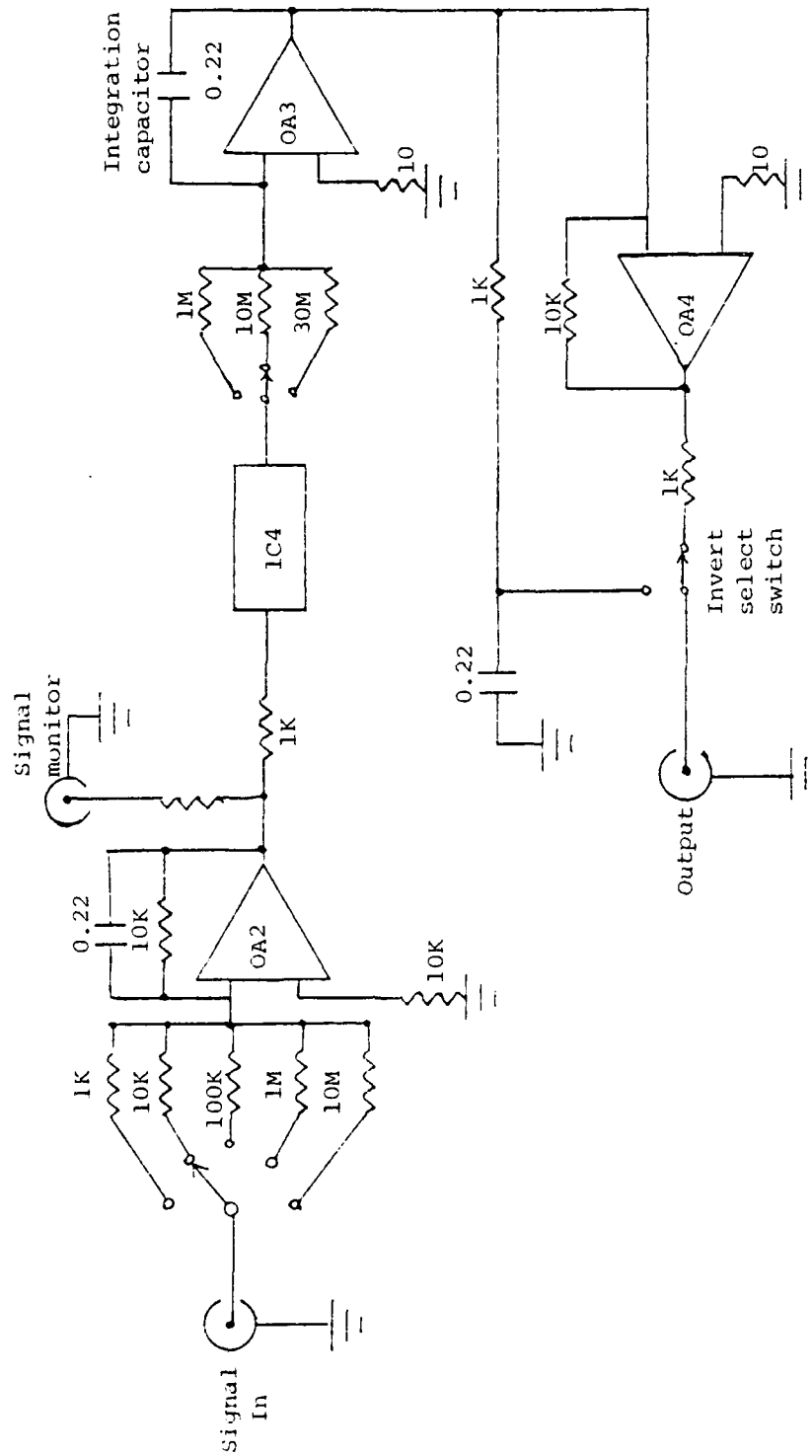


Figure 30: Gated integrator integration circuit. All resistors in ohms, all capacitors in μ F

LITERATURE CITED

1. Ralph Collacott, Chem. in Britain, 13-2, 60 (1977).
2. Spectroscopic Oil Analysis Program Laboratory, Mac Dill AFB, Tampa, FL., orientation visit, November 1979.
3. C. S. Saba and K. J. Eisentraut, Anal. Chem., 51, 1927 (1979).
4. R. L. Miller, L. M. Fraser and J. D. Winefordner, Appl. Spectrosc. No. 4, 477 (1971).
5. Joint Oil Analysis Program Technical Support Center, Naval Air Station, Pensacola, FL. 32508, 1979.
6. J. D. Winefordner and T. J. Vickers, Anal. Chem., 36, 161 (1964).
7. J. D. Winefordner and R. A. Staab, Anal. Chem., 36, 1165 (1964).
8. R. M. Dagnall, T. S. West and P. Young, Talanta, 13, 803 (1966).
9. C. Veillon, J. M. Mansfield, M. L. Parsons and J. D. Winefordner, Anal. Chem., 38, 204 (1966).
10. D. W. Ellis and D. R. Demers, Anal. Chem., 38, 1943 (1966).
11. R. M. Dagnall, K. C. Thompson and T. S. West, Anal. Chim. Acta, 36, 269 (1966).
12. D. C. Manning and P. Heneage, At. Abs. Newsletter, 7, 30 (1963).
13. M. P. Bratzel, Jr., R. M. Dagnall and J. D. Winefordner, Anal. Chim. Acta, 52, 157 (1970).
14. M. S. Cresser and T. S. West, Spectrochim. Acta, 25B, 101 (1970).
15. W. K. Fowler and J. D. Winefordner, Anal. Chem., 49, 944 (1977).
16. R. Smith, D. M. Stafford and J. D. Winefordner, Appl. Spectrosc. 25, 477 (1969).
17. D. J. Johnson, F. W. Plankey and J. D. Winefordner, Anal. Chem., 46, 1398 (1974).
18. D. J. Johnson, F. W. Plankey and J. D. Winefordner, Can. J. Spectrosc., 19, 151 (1974).

19. D. J. Johnson, F. W. Plankey and J. D. Winefordner, Anal. Chem., 47, 1739 (1975).
20. K. G. Brodie and J. P. Matousek, Anal. Chem., 43, 1557 (1971).
21. J. F. Alder and T. S. West, Anal. Chim. Acta., 58, 331 (1972).
22. S. Omang, Anal. Chim. Acta, 56, 470 (1971).
23. V. P. Borzov, B. V. L'vov and G. V. Plyuschch, Zh. Prikl. Spekt., 11, 217 (1969).
24. B. V. L'vov, Pure & Applied Chem., 23, 11 (1970).
25. M. D. Amos, Am. Lab., p. 33 (August 1970).
26. C. J. Molnar, R. D. Reeves, M. T. Glenn, J. R. Ahlstrom, J. Savory, and J. D. Winefordner, Appl. Spectrosc., 26, 606 (1972).
27. R. D. Reeves, C. J. Molnar, M. T. Glenn, J. R. Ahlstrom and J. D. Winefordner, Anal. Chem., 44, 2205 (1972).
28. F. S. Chuang and J. D. Winefordner, Appl. Spectrosc., 28, 215 (1974).
29. F. S. Chuang, B. M. Patel, R. D. Reeves, M. T. Glenn and J. D. Winefordner, Can. J. Spectrosc., 18, 6 (1973).
30. B. M. Patel, R. D. Reeves, R. F. Browner, C. J. Molnar and J. D. Winefordner, Appl. Spectrosc., 27, 171 (1973).
31. B. M. Patel and J. D. Winefordner, Anal. Chim. Acta, 64, 135 (1973).
32. D. A. Katskov, L. P. Kruglikova and B. V. L'vov, Anal. Abstr., 30, 3J59 (1976).
33. V. A. Razumov, Anal. Abstr., 33, 3J66 (1977).
34. Robert L. Vaughn, M. S. Thesis presented to the University of Florida, 1978.
35. N. Omenetto and J. D. Winefordner, Prog. Analyt. Atom. Spectrosc., 2, 1 (1979).
36. J. D. Winefordner, "Intensity Relationships in Analytical Optical Spectrometry," unpublished work for course CHM-6180, University of Florida, 1980.
37. J. D. Winefordner, V. Svoboda and L. J. Cline, CRC Crit. Rev. Anal. Chem., 1, 233 (1970).
38. J. D. Winefordner, Pure Appl. Chem., 33, 35 (1970).
39. T. C. O'Haver, Wavelength Modulation: Applications in Analytical Spectrometry, presented at the Fisher Award Symposium, ACS, 1973.

40. T. C. O'Haver, Anal. Chem., 41, 91A (1979).
41. M. S. Epstein and T. C. O'Haver, Spectrochim. Acta, 30B, 135 (1975).
42. E. H. Fisher, Laser Focus, p. 82 (November 1977).
43. G. D. Boutilier, B. D. Pollard, J. D. Winefordner, T. L. Chester and N. Omenetto, Spectrochim. Acta, 33B, 401 (1978).
44. F. S. Chuang and J. D. Winefordner, Appl. Spectrosc. 29, 412 (1975).
45. J. D. Winefordner, Trace Analysis: Spectroscopic Methods for Elements, John Wiley and Sons, NY (1976), p. 1.
46. IUPAC, Spectrochim. Acta, 33B, 247 (1978).
47. Designed by J. Bower, J. Bradshaw and T. Wynn, constructed by J. Bradshaw and T. Wynn, 1979.
48. J. D. Winefordner, S. G. Schulman and T. C. O'Haver, Luminescence Spectrometry in Analytical Chemistry, John Wiley and Sons, NY (1972), p. 127.
49. M. L. Parson, B. W. Smith and G. E. Bentley, Handbook of Flame Spectroscopy, Plenum Press, NY (1975), p. 74.
50. J. A. Krasowski and T. R. Copeland, Anal. Chem., 41, 1843 (1979).

BIOGRAPHICAL SKETCH

Thomas F. Wynn, Jr., was born on July 6, 1951, at the US Naval Hospital at Agana, Guam, Marianna Is. He graduated from Chofu Dependents High School, Tokyo, Japan (USAF) in 1969. He attended Troy State University, Troy, Al., from 1969 until his graduation in 1973 with a Bachelor of Science in chemistry cum laude.

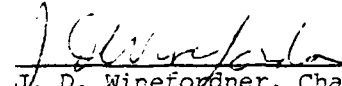
At the University, Thomas F. Wynn was inducted into Gamma Beta Phi, Kappa Omicron, Omicron Delta Kappa and the Arnold Air Society, all scholastic and leadership societies.

After graduation, he completed USAF undergraduate pilot training in 1973, and piloted C-130 aircraft worldwide until 1978, including a Southeast Asian tour. He was selected in 1978 by the Air Force Institute of Technology for graduate study in analytical chemistry. Upon completion of his studies, he will be assigned to the USAF Academy, Colorado Springs, Colorado, where his duties will include chemistry and flight instruction.

Thomas F. Wynn is a member of the American Chemical Society and the Analytical Division.

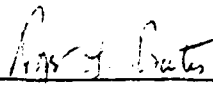
He is married to the former Deborah J. Stewart, and they have two children.

I certify that I have read this study and that in my opinion it conforms to acceptable standards of scholarly presentation and is fully adequate, in scope and quality, as a thesis for the degree of Master of Science.




J. D. Winefordner, Chairman
Professor of Chemistry

I certify that I have read this study and that in my opinion it conforms to acceptable standards of scholarly presentation and is fully adequate, in scope and quality, as a thesis for the degree of Master of Science



R. G. Bates
Professor of Chemistry

I certify that I have read this study and that in my opinion it conforms to acceptable standards of scholarly presentation and is fully adequate, in scope and quality, as a thesis for the degree of Master of Science.



G. M. Schmid
Associate Professor of Chemistry

This thesis was submitted to the Graduate Faculty of the Department of Chemistry in the College of Liberal Arts and Sciences and to the Graduate Council, and was accepted as partial fulfillment of the requirements for the degree of Master of Science.

March 1980

Dean, Graduate School

**DAT
FILM**